



Review

# Structure and Properties of High-Entropy Nitride Coatings

Vseslav Novikov <sup>1,\*</sup>, Nikita Stepanov <sup>2</sup>, Sergey Zherebtsov <sup>2</sup> and Gennady Salishchev <sup>2</sup>

- Joint Research Center "Technology and Materials", Belgorod State University, 308015 Belgorod, Russia
- Laboratory of Bulk Nanostructured Materials, Belgorod State University, 308015 Belgorod, Russia; stepanov@bsu.edu.ru (N.S.); zherebtsov@bsu.edu.ru (S.Z.); salishchev\_g@bsu.edu.ru (G.S.)
- \* Correspondence: novikov\_v@bsu.edu.ru

Abstract: The interest in nitride coatings based on high-entropy alloys (HEAs) has increased rapidly in the last decade. According to a number of papers, such high-entropy nitride (HEN) coatings have a single-phase structure and properties that significantly exceed those of simpler nitride systems. These properties include high hardness, wear resistance, oxidation resistance and thermal stability. It is believed that these distinctive properties are due to the high entropy of mixing, which increases with an increase in the number of elements in the composition. However, comparison with various binary and ternary systems shows that better properties are not typical of each HEA-based coating, and the effect of the number of elements competes with other factors that can make even more pronounced contributions to the structure and properties of the coating. Because of fragmentation of data on the structure and properties of high-entropy coatings, a unified concept of alloying is needed. This review compares the methods for obtaining HEN coatings, describes their structural features and analyzes the main properties, such as hardness, wear resistance and oxidation resistance, in order to establish an understanding of the influence of the number of elements and their role in the composition of coatings.

**Keywords:** high-entropy alloys; coatings; thin films; nitrides; PVD; structure; hardness; tribological properties



Citation: Novikov, V.; Stepanov, N.; Zherebtsov, S.; Salishchev, G. Structure and Properties of High-Entropy Nitride Coatings. *Metals* 2022, 12, 847. https://doi.org/10.3390/met12050847

Academic Editor: Jeff Th. M. De Hosson

Received: 19 April 2022 Accepted: 12 May 2022 Published: 16 May 2022

**Publisher's Note:** MDPI stays neutral with regard to jurisdictional claims in published maps and institutional affiliations.



Copyright: © 2022 by the authors. Licensee MDPI, Basel, Switzerland. This article is an open access article distributed under the terms and conditions of the Creative Commons Attribution (CC BY) license (https://creativecommons.org/licenses/by/4.0/).

## 1. Introduction

Nitride coatings obtained by PVD methods are widely used in machine tool [1] and aerospace industries [2] due to their high hardness and excellent wear and oxidation resistance. Examples include the wear-resistant coating for high-speed cutting tools and erosion-resistant coatings for compressor blades of gas turbine engines.

There is a wide range of nitride coatings that improve the functional properties of metal and non-metal materials [3]. The basis of this class of materials are mononitrides such as TiN [4], ZrN [5], CrN [6], etc. Such coatings have a hardness of 20–25 GPa [7] and high wear resistance but relatively low oxidation resistance (up to ~550-600 °C) [8]. One of the strategies to improve their thermal stability, oxidation resistance, and mechanical and tribological characteristics is the transition to multicomponent nitrides [9]. For example, the addition of transition metals, such as Al or Si (e.g., TiAlN [10], TiSiN [11], CrAlN [6], TiAlSiN [12] or TiAlCrYN [13]), can significantly improve physical and mechanical properties (hardness, wear resistance, oxidation resistance, etc.) of the coatings. Usually, a binary or ternary nitride of Al and/or transition metals (groups IV-VI of the periodic table) with carefully selected concentrations of elements are used to ensure optimal performance [9,14–17]. The concentration of the additional elements can be rather high for transition metals and/or Al or low in the case of Si (<10%) or Y (in the order of several %) due to possible property deterioration at higher concentrations [18,19]. Maximum hardness of some coatings can reach 30–50 GPa [6,10–13]; however, their service temperature does not exceed 900 °C because of the insufficient oxidation resistance at higher temperatures [13], which significantly limits potential application areas of the coatings.

Metals 2022, 12, 847 2 of 23

One of the possible ways to improve properties of multicomponent coatings is associated with the concept of high-entropy alloys (HEAs). Usually, HEAs are defined as alloys that contain at least five main components; the percentage of each species can vary from 5 to 35 at. % [20]. Due to high entropy of mixing (which increases with an increase in the number of elements), a stable single-phase solid solution can be expected to form in the alloy [21]. In fact, HEAs have the single-phase solid solution structure in only a limited number of systems [22]. According to various papers [23–25], some HEAs show very good combinations of strength, hardness, heat resistance and corrosion resistance in comparison with dilute alloys.

High-entropy nitride (HEN) coatings can also have a single-phase structure and properties that significantly exceed those of simpler nitride systems [26–33]; these properties include, for example, oxidation resistance [34], thermal stability [35], hardness [36] and wear resistance [37]. However, comparison with various binary [38–40] and ternary [41–43] nitrides suggests that increasing the number of components per se does not guarantee improvement in properties. Apparently, other factors such as the choice of the constitutive elements and/or deposition method and process parameters can have pronounced effects on the structure and properties of the coatings [44–48]. Note that the structure of HEN coatings can be more complex than random solid solutions [44,45]. However, despite the large number of published works, the links between the preparation methods, composition, structure, and properties of HEN coatings still have not been fully established. This review aims to provide valuable insight into the composition–structure–properties relationships in multicomponent nitride coatings.

## 2. Methods of Preparation of High-Entropy Nitride Coatings

The choice of deposition method that ensures the uniformity of composition, single-phase structure and high quality of a high-entropy nitride coating is a challenge. Among many options of physical vapor deposition (PVD), vacuum-arc deposition [49] and magnetron sputtering [46,50,51] are the most effective and wide-spread approaches. In these methods, metal targets are sputtered in a nitrogen atmosphere or in an  $Ar + N_2$  gas mixture. Several types of targets can be used: sputtering of a solid multicomponent target [52], simultaneous sputtering from several elementary targets [53] and sputtering of mosaic targets (applicable for the magnetron method) [54,55]. High-entropy alloys' multicomponent targets are usually fabricated by vacuum-arc melting [56] or using powder metallurgy methods, including cold or hot pressing [57,58], spark plasma sintering [59] and some others.

Two groups of metals can be distinguished depending on their inclination towards nitride formation in HEN coatings obtained by sputtering targets: (i) low (Mn, Fe, Co, Ni) or zero (Cu) tendency [57,60–62] and (ii) high tendency (transition metals of IV–VI groups (Ti, Zr, Hf, V, Nb, Ta, Cr, Mo, W)) [63–65]. HEN coatings of metals of the first group usually show poor mechanical properties and a tendency to form an amorphous or bcc structure. These properties can be related to an insufficient nitrogen content, low strength of the metal–nitrogen bond and thermodynamic instability of such nitrides [58,62,66]. Transition metals of groups IV–VI in the coatings provide higher strength of the metal–nitrogen bonds, a tendency to form a crystal structure of the NaCl type and high hardness. Both Al and Si can also form strong covalent bonds with nitrogen, but in multicomponent coatings, these elements promote the formation of additional phases with an hcp [67] or amorphous [68] structure. Coatings based on transition metals of groups IV–V (Ti, Zr, Hf, V, Nb, Ta) are promising due to high hardness levels [36]. In addition, they also have good mutual solubility of binary nitrides promoted in the formation of a single-phase structure stable up to temperatures above 1300 °C [69].

The structure and hardness of HEN coatings based on groups IV–V metals significantly depend on the method of deposition (Table 1). The Ti–Zr–Hf–V–Nb–N system coatings [36,44,63,70,71] were obtained using either magnetron sputtering of three elementary targets (Hf, Ti, V) and one mosaic Nb/Zr [44], or vacuum-arc sputtering of a multicomponent cathode [36,63,70,71]. The compositions of coatings obtained by the

Metals **2022**, 12, 847 3 of 23

vacuum-arc method significantly depended on the deposition parameters (nitrogen pressure, bias potential on the substrate). The nitrogen content in [63] varied in the range from 36 to 51 at. %. The percentage of other components also varied significantly ( $C_{Ti}$  = 16–25 at. %,  $C_{V}$  = 1–6 at. %,  $C_{Zr}$  = 6–17 at. %,  $C_{Nb}$  = 6–18 at. %,  $C_{Hf}$  = 4–11 at. %), probably due to secondary selective sputtering [72] or chemical inhomogeneity of the initial HEA target. However, the usage of several magnetrons with elemental targets has allowed the ability to produce coatings with the desired compositions. For example, the content of Hf in the coating obtained by magnetron sputtering [44] varied from 0 to 18 at. % (due to different Hf target currents), while the ratio of other metal elements did not change significantly. For example, in a coating with  $C_{Hf}$  = 3 at. %, the concentration of other elements was  $C_{Ti}$  = 14 at. %,  $C_{V}$  = 13 at. %,  $C_{Zr}$  = 17 at. % and  $C_{Nb}$  = 10 at. %, and in the coating with  $C_{Hf}$  = 18 at. % was  $C_{Ti}$  = 10 at. %,  $C_{V}$  = 10 at. %,  $C_{Zr}$  = 13 at. % and  $C_{Nb}$  = 6 at. %. The nitrogen content in both coatings was 43–44% at.%.

Despite the differences in chemical composition, the phase composition of the coatings was rather similar. In the coatings reported in [36,63,70,71], only one face-centered cubic (fcc) phase was found for all compositions, while in [44] the coatings are shown to have either a single-phase fcc structure or two-phase fcc + bct (body-centered tetragonal) one, depending on the Hf content. However, since the bct and fcc phase peaks at the X-ray diffraction (XRD) pattern can overlap each other, precise identification of the phase composition requires more detailed structural characterization. That is why in some coatings described in the literature as single-phase ones, additional phases can be present. These potentially multiphase structures should be taken into account when analyzing the structure and properties of the coatings.

The structure of the coatings also depends significantly on the preparation method (Table 1). Coatings obtained by the magnetron method [44] have a fine-grained structure (tens of nanometers) nearby the interface with the substrate; a coarse columnar structure (several hundreds of nanometers height  $\times$  100 nm width) forms towards the coatings surface. The average grain size measured by X-ray diffraction analysis was several tens of nanometers. A similar structure was observed in coatings obtained by the vacuum-arc method [70]. The transition from a fine-grained structure to the columnar one was observed at a distance of 2  $\mu$ m from the substrate (the total coating thickness was 10–12  $\mu$ m). The average grain size calculated from X-ray diffraction for these coatings was 18–42 nm. For each deposition method, the structure of the coatings is mainly determined by parameters of the process, i.e., temperature of the substrate, bias potential or nitrogen pressure. Depending on the exact process parameters, HEN coatings can have both a homogeneous structure (columnar [73], equiaxed [69] or amorphous [66]) or gradient structure comprising amorphous or fine-grained and columnar layers [65,74].

Despite the similarity in the HEN coatings' structure obtained by different methods and with different parameters (i.e., [44] or [70]), their hardness can vary significantly (Table 1). Moreover, indentation methods also have a pronounced effect on the obtained hardness values. For example, in [63], microindentation returned hardness values of 21–27 GPa depending on the deposition parameters, while nanohardness values were in the range of 36–44 GPa. Similarly, in [44] (the coating was obtained by magnetron sputtering) and [70] (vacuum-arc sputtering), the respective maximum micro- and nanohardness values were 19 GPa [44] and 53 GPa [70]. Meanwhile, the maximum nanohardness of the coatings obtained by the vacuum-arc method in [63] reached 44 GPa, which is significantly higher than the values (19 GPa) of coatings produced by the magnetron method [44].

Residual stresses can significantly affect the hardness of the coatings [75,76]. Coatings obtained by the vacuum-arc method in [63,70] have relatively high compressive stresses (up to -3.7 GPa), while those in coatings produced by the magnetron method [44] did not exceed -0.23 GPa. Residual stresses depend on the specific substrate/coating couple [77] and deposition parameters. For example, bias potential applied to the substrate or high-energy ion bombardment also increases residual stresses in the coatings. An increase in the bias potential from -50 V to -200 V during vacuum-arc sputtering increased

Metals **2022**, 12, 847 4 of 23

the hardness values of (TiZrHfVNb)N coatings from 21 to 28 GPa [63]. Another factor influencing the level of residual stresses is the partial pressure of nitrogen during the deposition process. For instance, the residual stresses in (TiZrHfVTa)N coatings obtained by magnetron sputtering varied in the range from -1.6 GPa to -2.5 GPa depending on the Ar/N2 ratio [69]. The hardness of coatings correlated with the residual stresses and increased from 30 GPa to 34 GPa, respectively.

Coatings obtained by the vacuum-arc method show the highest hardness (Table 1). It is known [78] that a high degree of gas ionization during vacuum-arc deposition leads to densification of the growing film due to the increased mobility of adsorbed atoms, which ensures high mechanical properties of the coatings. However, during deposition of (TiVCrZrHf)N HEN coatings using magnetron sputtering [65], an amorphous structure was formed near the interphase boundary due to heating of the substrate and a corresponding increase in the mobility of adsorbed atoms; a dense columnar crystalline structure was observed close to the substrate surface. Such a coating has a maximum hardness of 48 GPa, which is comparable to the hardness of some coatings obtained by the vacuum-arc method (Table 1). Thus, for both the vacuum-arc and magnetron methods, a significant difference in the structure and properties of coatings was mainly caused by different parameters of the deposition process.

## 3. Structure of High-Entropy Nitride Coatings

HEN coatings are based on interstitial nitrides of groups IV–VI metals [79]. In addition, covalent nitrides of Al and Si can be presented [80]. A complex combination of covalent and metallic bonds is typical of interstitial nitrides. Structure and electronic properties of ternary nitrides  $Ti_xTa_{1-x}N$  and  $Ti_xZr_{1-x}N$  were calculated in [81]. Despite the similar crystal structure of ternary compounds  $Ti_xMe_{1-x}N$  and  $Ta_xMe_{1-x}N$  (Me = Ti, Zr, Hf, Nb, Ta, Mo, W), the configuration of valence electrons significantly affects the bond with nitrogen. The charge density of  $Ti_{50}Zr_{50}N$  exhibits metal-like features, as in TiN or ZrN, while Ti<sub>50</sub>Ta<sub>50</sub>N is rather characterized by a directional bond between Ti and Ta atoms, suggesting covalent bonds and higher material hardness. Incorporating Ta in  $Ti_{1-x}Ta_xN$ and Ta<sub>1-x</sub>Zr<sub>x</sub>N leads to a shift of the bonding state region away from the Fermi level, suggesting a stronger covalent bonding. This results in a considerably higher bulk modulus of TaN (B = 330–370 GPa) in comparison with TiN (B = 270 GPa) or ZrN (B = 245 GPa) [82]. The hardness of  $Ti_xTa_{1-x}N$  and  $Ta_{1-x}Zr_xN$  coatings reported in [82] reaches 42 GPa and 32 GPa, respectively, while the hardness of  $Ti_xZr_{1-x}N$  does not exceed 25 GPa. However, one must keep in mind that the microstructure of the coating can also affect the hardness. In contrast to interstitial nitrides, differences in electronegativity and atomic size between nitrogen and another element in covalent nitrides are small, and their bond is essentially covalent [80].

The common structural element of fcc nitrides of groups IV-V transition metals is a M<sub>6</sub>N octahedron with a nitrogen atom in the center [83] (Figure 1a). Stability of the octahedron depends on the  $r_N/r_M$  ratio (radii of nitrogen and metal atoms, respectively), since changes in this value result in transformation into trigonal prismatic group M<sub>6</sub>N. Due to the formation of structural elements other than the M<sub>6</sub>N octahedron, the fcc structure of nitrides gradually destabilizes with an increase in the group number or with an increase in the periodic number within the group. For example, group IV nitrides (TiN, ZrN and HfN) form a NaCl-type structure. In group V all three metals (V, Nb, Ta) also form stoichiometric nitrides with an fcc lattice. However, fcc-VN below -68 °C transforms into the tetragonal modification, fcc-NbN below ~1320 °C turns into the hexagonal (hcp) modification and fcc-TaN at temperatures below 1920 °C congruently transforms into the hexagonal modification [83]. In group VI (Cr, Mo, W), fcc nitrides gradually become less stable. Face-centered cubic CrN is a compound with a very narrow homogeneity range around stoichiometric composition and reduced thermochemical stability at low temperatures. Below ~7 °C, CrN transforms into a tetragonal compound [83]. Molybdenum nitride with an fcc lattice forms at only a stoichiometry close to Mo<sub>2</sub>N and then transforms

Metals **2022**, 12, 847 5 of 23

between 400 and 850 °C (depending on the composition) into a tetragonal modification with an ordered arrangement of nitrogen atoms in interstices. The stable forms of covalent Al and Si nitrides are phases with an hcp lattice [83].

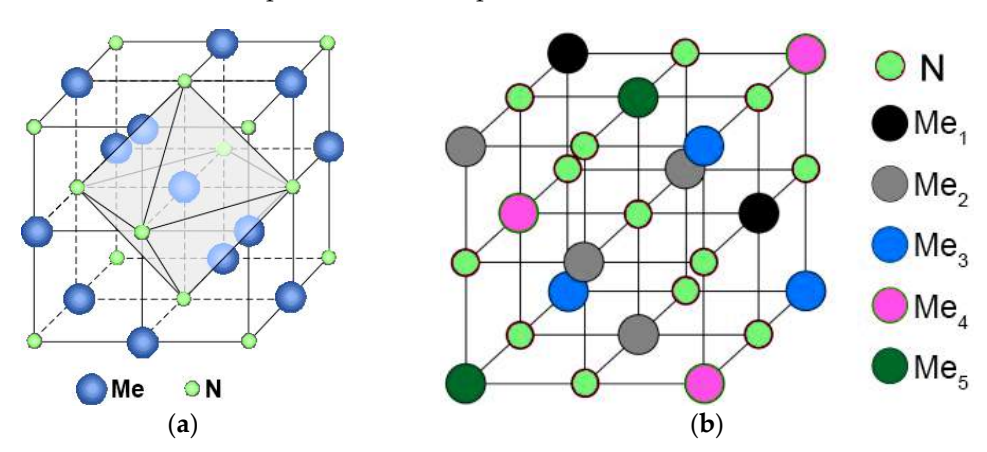


Figure 1. Face-centered cubic structure of (a) binary and (b) high-entropy nitrides.

However, in the case of multicomponent nitride coatings, as shown earlier, the NaCl-type phase with a disordered metal fcc sublattice is predominantly formed [84] (Figure 1b). An addition to the metal sublattice of various metallic elements with different electronic structures and atomic radii causes local distortions in HEN coatings' lattices (like that in high-entropy alloys) [85] and influences mechanical properties significantly [86]. Meanwhile, there are rather limited data on the structure of high-entropy nitrides and the contributions of various types of chemical bonding [26–33].

Yet, some results for high-entropy carbides were obtained using first-principle calculations [87]. It worth noting that among all compounds formed by atoms of transition metals and light elements (H, B, C, N, O), only carbides have crystal structures, phase relationships, bond types, electrical and magnetic properties like those of nitrides. This proximity can be caused by similar electronic structure, size and electronegativity of carbon and nitrogen atoms. Local lattice distortions, stability, electronic structure, bulk elastic modulus and thermodynamic properties of multicomponent (NbTaZr)C, (NbTaTiZr)C, (NbTiVZr)C, (HfNbTaTiZr)C and (MoNbTaVW)C carbides were studied in [87]. It was shown that the crystal lattice distortions do not depend on the number of elements but rather increase with an increase in the mismatch of atomic sizes for carbides of groups IV–V metals (the carbides can also contain some group VI metals (Mo, W) that usually do not form carbides with a stable NaCl structure). The covalent bond was found to become stronger from Zr/Ti-C to V/Nb/Ta-C [87]. This result, together with the analysis of the bulk elastic modulus for binary and multicomponent carbides, suggests a more pronounced influence of electronic interaction on mechanical properties of carbides and nitrides in comparison with the effects of solid solution strengthening caused by lattice mismatch. Calculations also show that lattice distortion results in a negative enthalpy of mixing for most high-entropy carbides [87]. Therefore, these high-entropy carbides can be stabilized by enthalpy solely. This conclusion differs from many other works, in which a decisive contribution of the configurational entropy to the stabilization of a single-phase state was stated [86,88–90].

The effect of the number of elements on the structure of high-entropy nitrides was studied in [89,91] for 8-component (TiVZrNbMoTaAlSi)N and 11-component (TiVCrZrNbMoHfTaWAlSi)N coatings. A multi-phase structure would be expected to form in these alloys containing elements with different atomic sizes and types of chemical bonds. The metallic elements also form mononitrides with different types of crystal lattice. However, like high-entropy coatings with fewer elements, these coatings had a single-phase structure with an fcc lattice (in the 11-component coating (TiVCrZrNbMoHfTaWAlSi)N with a nonstoichiometric nitrogen composition, an insignificant amount of the hcp phase was also formed).

Metals **2022**, 12, 847 6 of 23

This effect was ascribed to a large lattice mismatch among binary nitrides (eg, AlN and ZrN) that creates high mixing enthalpy of many complex nitride compounds and promotes phase separation [92]. According to XRD results, the coatings still have one fcc phase without traces of the hcp phase when the nitrogen content in the coating reaches 42.1 at.%. Therefore, the single-phase structure of HEN coatings can survive even in 11-component systems; however, it is still unclear if it remains stable at elevated temperatures.

The thermal stability of high-entropy coatings (Ti<sub>0.19</sub>Zr<sub>0.18</sub>Hf<sub>0.22</sub>V<sub>0.18</sub>Ta<sub>0.2</sub>)N was studied during annealing in vacuum at temperatures up to 1500 °C [69]. The coatings contained only interstitial nitrides of groups IV-V metals, which are most prone to the formation of a single-phase structure of the NaCl type. Atom probe tomography (APT) revealed a random distribution of the elements in the coating (Figure 2). According to first principles calculations, at temperatures above 1029  $^{\circ}$ C, the Gibbs energy of fcc-(Hf,Ta,Ti,V,Zr)N is lower than those of the competing components considered in this case (i.e., fcc-(Hf,Zr)N and fcc-(Ta,Ti,V)N) (Figure 3). Experiments showed that the single-phase state with the fcc structure and uniform distribution of all elements is retained even after annealing at 1300 °C. However, TaN and VN readily lose nitrogen during annealing in vacuum at higher temperatures [93,94], resulting in the formation of phases with a hexagonal structure. Thus, the onset of fcc-(HfTaTiVZr)N decomposition with the formation of hcp-(Ta,V)<sub>2</sub>N can be suggested at ~1350 °C. Moreover, after vacuum annealing at 1500 °C, the appearance of (Ta,V)-enriched regions with N concentrations <38 at. % was reported (Figure 2). Thus, it can be suggested that as long as nitrogen loss is prevented, even higher thermal stability can be achieved for such coatings.

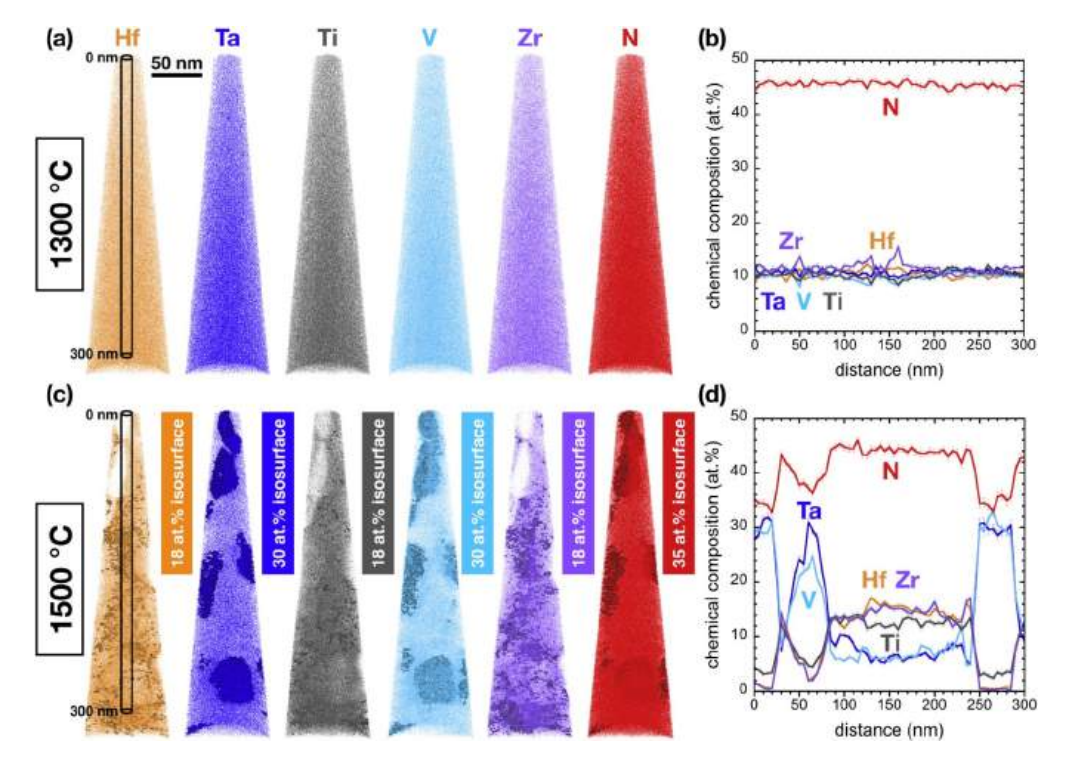


**Figure 2.** Local chemical composition of our (Hf,Ta,Ti,V,Zr)N prepared with  $fN_2 = 45\%$  at the nanometer scale. (a) Reconstruction of Hf, Ta, Ti, V, Zr and N atomic positions after vacuum annealing at 1300 °C. (b) Concentration profile of the cylindrical region indicated in (a). (c) Reconstruction of Hf, Ta, Ti, V, Zr and N atomic positions after vacuum annealing at 1500 °C. (d) Concentration profile of the cylindrical region indicated in (c). Reproduced from [69].

Metals **2022**, 12, 847 7 of 23

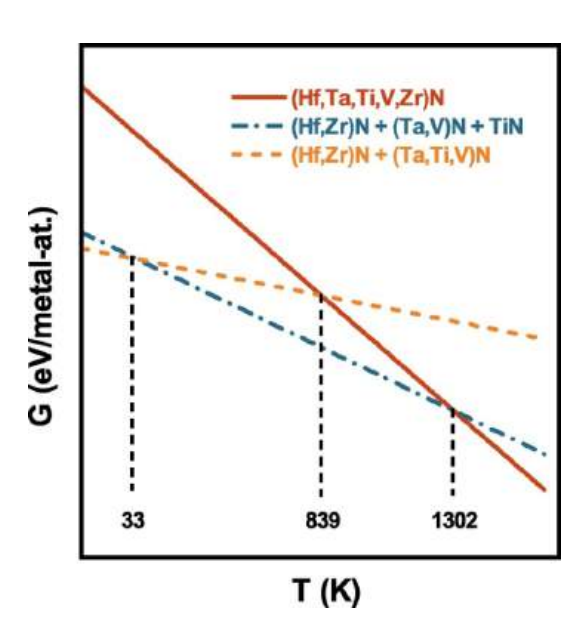


**Figure 3.** Schematic G-versus-T curves for a high-entropy metal-sublattice fcc-(Hf,Ta,Ti,V,Zr)N and the possible products (fcc-(Hf,Zr)N, fcc-(Ta,V)N and fcc-TiN and fcc-(Hf,Zr)N and fcc-(Ta,Ti,V)N). Reproduced from [69].

The effect of Al (which has covalent bonds with nitrogen) on the structure and stability of high-entropy ( $Al_{0.17}Ti_{0.41}V_{0.14}Cr_{0.04}Nb_{0.24}$ )N and ( $Al_{0.31}Ti_{0.34}V_{0.12}Cr_{0.06}Nb_{0.17}$ )N coatings obtained by vacuum-arc sputtering was examined in [67]. Hexagonal AlN readily dissolves in an fcc lattice. For example, (AlTi)N solid solutions have an fcc lattice until ~70% of AlN and an hcp lattice above 70% of AlN [95]. The (AlTiVNbCr)N coatings had the fcc NaCl-type structure with positive enthalpy of mixing (0.06 eV/atom). Ab initio calculations have demonstrated higher thermodynamic stability of the synthesized (AlTiVNbCr)N solid solutions with respect to their constituent binary compounds, thereby suggesting entropy-caused stabilization at temperatures above 727 °C. However, during high-temperature annealing, multicomponent (AlTiVNbCr)N solid solutions show limited thermal stability and decomposed into equilibrium mixtures of wurtzite B4 AlN and cubic B1 (TiVNbCr)N phases (Figure 4).

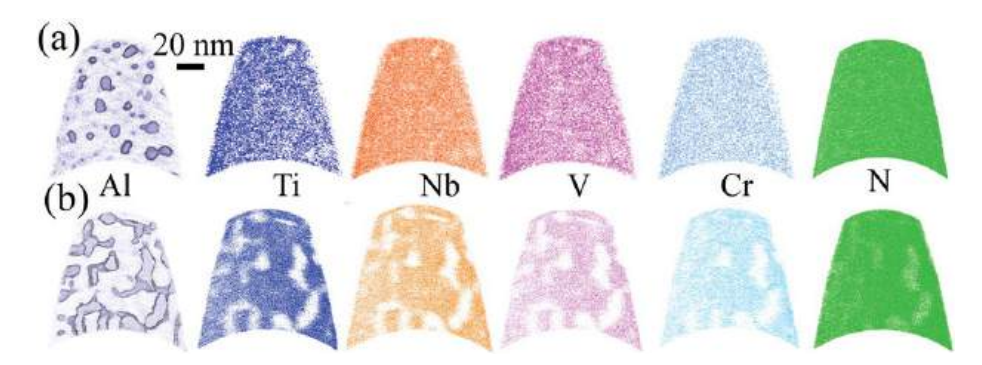


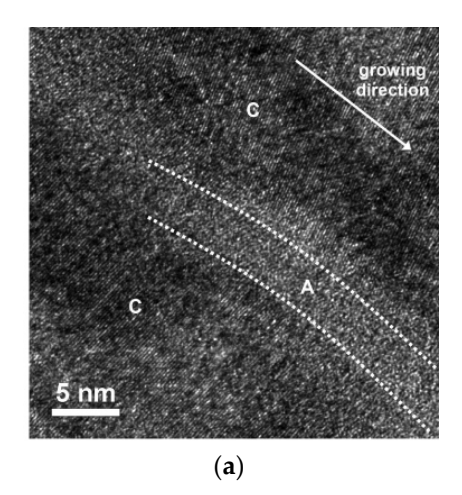
**Figure 4.** APT reconstruction (5 nm thin slice) revealing elemental distribution after annealing at  $1100\,^{\circ}$ C, 2 h for (a)  $(Al_{0.17}Ti_{0.41}V_{0.14}Cr_{0.04}Nb_{0.24})N$  and (b)  $(Al_{0.31}Ti_{0.34}V_{0.12}Cr_{0.06}Nb_{0.17})N$ . For Al, APT analysis also shows isoconcentration surface at 25 at.%. Reprinted with permission from ref. [67]. Copyright 2017 Elsevier.

The results obtained suggest the metastability of the homogeneous solid solution structure in HEN coatings. In addition, the solid solution was not stabilized by entropy of mixing, which should increase with temperature. Moreover, differential scanning calorimetry showed that the temperatures corresponding to hcp-AlN precipitation are rather similar for both  $(Al_{0.17}Ti_{0.41}V_{0.14}Cr_{0.04}Nb_{0.24})N$  and  $Ti_{0.8}Al_{0.2}N$ , despite their significant difference

Metals **2022**, 12, 847 8 of 23

in configurational entropy (1.41 and 0.5  $K_B$ /atom, respectively, where  $K_B$  is the Boltzmann constant). These results further emphasize that the thermodynamic stability of a multicomponent solid solution is not determined by the entropy value [96].

The effect of Si on the phase composition and microstructure of HEN coatings was studied in [68,97–100]. The solubility of silicon in fcc nitrides is limited in simple systems like TiSiN [101] as well as in high-entropy coatings. According to [97], the formation of a single-phase structure in (AlCrTaTiZrSi)N coatings obtained by magnetron sputtering was observed when Si percentage was <7.9 at.%. At 7.9 at. % of Si, an amorphous covalent SiNx phase was formed along the crystallite boundaries (Figure 5a). When the silicon content reaches 10.2 at. %, a dual-phase nanocomposite structure of fcc nanocrystalline and amorphous phases (Figure 5b) is observed. Layers of the amorphous phase separate nitride grains and restrict their growth [68]. The threshold concentrations of Si required for the nanocomposite structure formation varies [68,97–100] depending on solubility of silicon in different nitrides [98,102–104]. In addition, the amorphous phase was not observed in some Si-containing systems [89,91,105] probably due to small thickness amounts that complicate identifying by such methods as EDS and EELS.



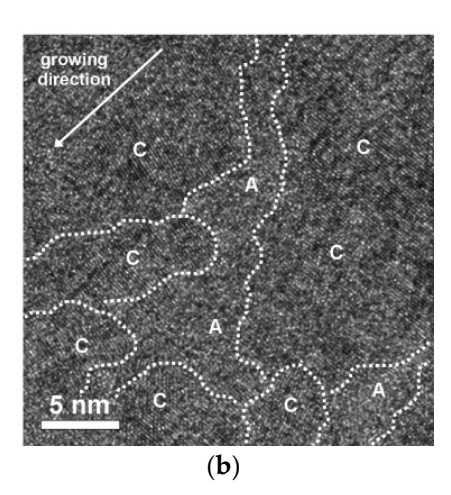


**Figure 5.** HRTEM lattice images of two nitride films with Si contents: (a) 7.9 at. % and (b) 10.2 at. % (A: amorphous region; C: crystalline region). Reprinted with permission from ref. [97]. Copyright 2011 IOPScience.

Thermal stability of (AlCrNbTaTi)N and (AlCrNbTaTiSi)N coatings (Si concentration was 6.4–15.0 at. %) was studied in [100]. The second coating had a single fcc phase structure at Si concentration < 9.8 at.%, similar to the first one. Segregations of silicon at the crystallite boundaries in the (AlCrNbTaTiSi)N coating with Si  $\geq$  9.8 at.% can indicate the formation of an amorphous phase. Annealing in vacuum at temperatures up to 900 °C for 10 min did not change the structure of the coatings. Annealing of the (AlCrNbTaTi)N coating at 1000 °C resulted in the formation of a covalent hcp-AlN nitride in the initial fcc phase. In the silicon-containing (AlCrNbTaTiSi)N coating, the structure was more stable. The decomposition of the solid solution was observed only at 1200 °C in samples containing 12.0 and 15.0 at.% of Si (at lower amounts of Si coating delaminated). The formation of hcp-AlN, Nb<sub>0.16</sub>Ti<sub>0.84</sub> and Al<sub>3</sub>Ti intermetallics, Ti<sub>5</sub>Si silicide and nitrogen-depleted Cr<sub>2</sub>N and Nb<sub>2</sub>N phases was found. The tendency of CrN and TaN mononitrides to release N<sub>2</sub> and form Cr<sub>2</sub>N at temperatures above 900 °C and Ta<sub>2</sub>N at 1100 °C was supposed to be the main factor limiting the phase stability of both coatings [94,106].

Thus, HEN coatings can retain a single-phase structure with an increase in the number of metallic elements up to 11 [89]. However, the available literature data do not allow any conclusions on the effect of configurational entropy on the stabilization of the coatings' structure. The stability of such solid solutions at high temperatures is mostly limited by the nitrogen evaporation temperatures. These temperatures are directly related to the temperatures of nitrogen loss in the corresponding mononitrides. Thus, thermal stability of

Metals **2022**, 12, 847 9 of 23

HEN coatings should not exceed that of similar triple or quadruple nitride coatings. When Al or Si, which have strong covalent bonds with nitrogen, are added to the coatings, the formation of amorphous and/or hcp phases is expected. The major requirement for the formation of a stable solid solution is the usage of metallic elements of groups IV–V, which tend to form MeN nitrides with a NaCl-type structure.

## 4. Properties of High-Entropy Nitride Coatings

### 4.1. Hardness

HEN coatings can offer significant improvements in properties when compared with binary and ternary nitrides [27–37], especially high hardness and elastic modulus.

An analysis of the available literature data suggests that the hardness and elastic modulus increase of the nitride coatings tend to increase with the number of components (Figure 6). Indeed, hardness of high-entropy coatings was found to be higher than those of binary and ternary nitrides [36,55,63,66,88,107]. Examples of HEN coatings with very high hardness are (AlCrTiVZr)N—42 GPa [55], (TiZrNbAlYCr)N—47 GPa [107] and (TiHfZrVNb)N—65 GPa [36]. However, as noted above (Section 2), this situation is typical for coatings composed of nitride-forming elements; alloying with non-nitride-forming elements decreases the hardness. In the latter case, the hardness of HEN coatings can be even lower than that of binary nitrides [60,108]. The effect of elements that are not prone to nitride formation (Mn, Fe, Co, Ni, Cu) on hardness of high-entropy coatings is shown in Table 2. The first four metals form intermediate nitrides that decompose readily due to low chemical stability [109]. Copper does not react directly with nitrogen up to extremely high pressures and temperatures [110]. For comparison, coatings containing nitride-forming elements solely are shown in Table 3. Obviously, the addition of even one non-nitride-forming element (such as Ni) leads to a significant decrease in hardness. Meanwhile, (TiZrNbTaFe)N coatings have a high hardness of 36 GPa, exceeding that of many binary nitrides. This result may be caused by (i) the prevalence of strong nitride-forming elements (Table 2) and (ii) the formation of dense nanocrystalline structures with high residual stresses due to highenergy ion bombardment [76]. It should be noted that the separation based on the presence of non-nitride-forming elements is valid for any nitride coatings. Thus, the maximum hardness of (CrFeCo)Ni coatings was found to be 11 GPa [111], which is approximately two times lower than the hardness of binary CrN [16,38,112].

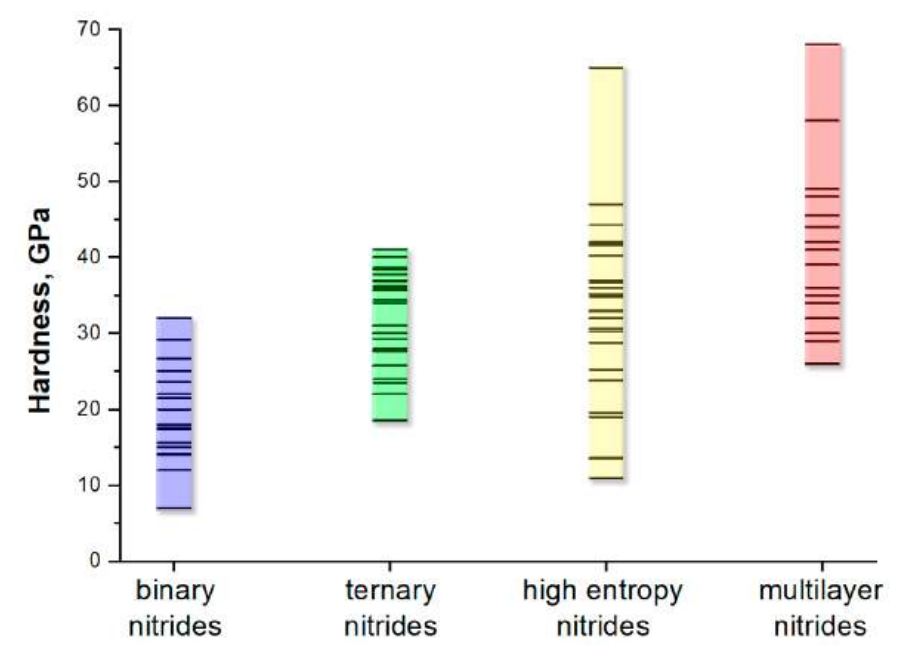


**Figure 6.** Hardness ranges of binary, ternary, high entropy and nanocomposite multilayer nitride coatings. The horizontal lines mark some hardness values given in different publications [15–193].

Metals **2022**, 12, 847 10 of 23

**Table 1.** Structure and hardness of coatings based on groups IV and V metals, depending on the method of deposition.

System of Coating	Method of Deposition	Target	Material/Temperature of Substrate, °C/Bias, V	Thickness, µm	Structure of Coating	Hardness	References
(TiZrHfVNb) <sub>0.56</sub> N <sub>0.44</sub>	DC magnetron sputtering	elemental Hf, Ti, V + mosaic Nb <sub>0.5</sub> Zr <sub>0.5</sub>	Si, SiO <sub>2</sub> , α-Al <sub>2</sub> O <sub>3</sub> <sup>1</sup> /520 °C/100 V	1.2	FCC + BCT	9–19 GPa <sup>2</sup>	[44]
$(TiZrHfVNb)_{1-x}N_x$ $x = 0.36-0.5$	cathode-vacuum-arc deposition	HEA Ti-Zr-Hf-V-Nb	Steel AISI 1045/400 °C/50—230 V	4–5	FCC	36–44 GPa <sup>2</sup> 19–30 GPa <sup>3</sup>	[63,71]
(TiZrHfVNb)N	cathode-vacuum-arc deposition	HEA Ti-Zr-Hf-V-Nb	Steel 12X18H9T (AISI 321)/40—200 V	6	FCC	57–66 GPa <sup>3</sup>	[36]
$(Ti_{0.19}Zr_{0.18}Hf_{0.22}V_{0.18}$ $Ta_{0.23})N$ $C_N = 47-50$ at. %	DC magnetron sputtering	equiatomic HEA Ti-Zr-Hf-V-Ta	Si, $\alpha$ -Al $_2$ O $_3$ $^1$ , low alloy steel/440 $^{\circ}$ C/50 V	2.2–4.7	FCC + undetermined phase (low content)	30–34 GPa <sup>2</sup>	[69]
(TiZrHfNbTa) <sub>0.5</sub> N <sub>0.5</sub>	DC magnetron sputtering	elemental Ti, Zr, Nb, Hf, Ta	Steel C45 and M2/300 °C/100 V	2	FCC	33 GPa <sup>3</sup>	[143]
$(Ti_{0.21}Zr_{0.26}Hf_{0.19}V_{0.12}\ Nb_{0.22})N$	cathode-vacuum-arc deposition	HEA Ti-Zr-Hf-V-Nb	200 V	10–12	FCC	53 GPa <sup>3</sup>	[70]
(TiVCrZrHf) N	RF magnetron sputtering	equiatomic HEA Ti-V-Cr-Zr-Hf	p-Si (100)/RT—450 °C/100 V	1–1.2	FCC	30–48 GPa <sup>3</sup>	[65]

<sup>&</sup>lt;sup>1</sup> the substrate was used to measure the hardness. <sup>2</sup> nanoindentation. <sup>3</sup> microindentation.

Metals 2022, 12, 847 11 of 23

**Table 2.** The effect of elements with a low tendency to form nitrides (Mn, Fe, Co, Ni, Cu) on hardness of high-entropy coatings.

Composition of High-Entropy Coatings	Hardness, GPa	Elements with a Low Tendency to Form Nitrides	Elements with a High Tendency to Form Nitrides	References
(Al0.5CoCrCuFeNi)59N41	10	Co, Cu, Fe, Ni	Al, Cr	[60]
(AlCoCrCu0.5FeNi)N	10	Co, Cu, Fe, Ni	Al, Cr	[108]
(AlCrMnMoNiZr)N	12	Mn, Ni	Al, Cr, Mo, Zr	[185]
(FeCoNiCuVZrAl)N	12	Fe, Co, Ni, Cu	V, Zr, Al	[61]
(FeCoNiCrCuAlMn)N	12	Fe, Co, Ni, Cu, Mn	Al, Cr	[60]
(AlCrNiSiTi)82N18	15	Ni	Al, Cr, Si, Ti	[186]
(CoCrCuFeNi)N	15	Co, Cu, Fe, Ni	Cr	[57]
(AlCrMoNiTi)Nx	15	Ni	Al, Cr, Mo, Ti	[58]
(TiZrHfNiCuCo)N	17	Ni, Cu, Co	Ti, Zr, Hf	[188]
(FeMnNiCoCr)N	17	Fe, Mn, Ni, Co	Cr	[62]
(Al0.5CrFeNiTi0.25)Nx	21	Fe, Ni	Al, Cr, Ti	[187]
(TiZrNbTaFe)N	36	Fe	Ti, Zr, Nb, Ta	[76]

**Table 3.** Hardness of coatings containing only elements with a high tendency to form nitrides.

System of Coating	Hardness, GPa	References
CrN	18–27	[16,38,112]
ZrAlN	24	[189]
(TiAlCr)N	28	[191]
(TiZrHf)N	32	[192]
CrAlN	36	[16]
(AlCrSi)N	40	[190]
VAIN	41	[43]
(AlTiSi)N	50	[190]

In general, the hardness increases with an increase in the number of components. This effect was demonstrated for coatings obtained using the same procedures. For example, in [15], binary TiN, CrN and ZrN and ternary TiCrN, TiZrN, TiAlN and TiVN nitride coatings were obtained using the same deposition parameters with the identical percentages of Ti and other metals in cathode material. The hardness levels of binary nitrides were TiN—2000 HV, CrN—1400 HV and ZrN—1500 HV. The hardness levels of triple nitrides were significantly higher: TiCrN and TiZrN—3000 HV, TiAlN—3100 HV and TiVN—2400 HV. The further increase in the number of elements was considered in [14], where a series of coatings with different numbers of elements were produced: TiN, TiAlN and TiAlCrN. Their hardness levels were 1222 HV, 1916 HV and 3033 HV, respectively. Such an increase in hardness is not only due to stronger solid solution strengthening, but also can be attributed to the stronger covalent bonds introduced by Al [16]. Moreover, the formation of a nanocomposite amorphous-crystalline microstructure can also result in a significant increase in hardness, as it was shown for CrAlN coatings with  $\sim$ 5 nm crystallites uniformly distributed in the amorphous matrix [113].

In HEN coatings, the hardness varies in a wider range (Figure 6). Probably, with an increase in the number of elements in the system, the number of combinations of different factors (different radii of metal atoms, the tendency to form nitrides, types of the chemical bonding) that determine the properties of coatings also increases. The overlapping of these factors with different methods (or even different parameters) for the deposition can result in considerably different compositions and structures of the coatings. For example, the hardness of (TiZrHfVNb)N coatings, obtained by various methods, varied from 9–19 GPa [44] to 36–44 GPa [63] and 60–65 GPa [36]. However, the hardness of 65 GPa (the record-breaking hardness values for nitride coatings) claimed in [36] is significantly different from all the other results and needs additional confirmation. Low hardness values

Metals **2022**, 12, 847 12 of 23

( $\leq$  20 GPa) were mostly associated with a significant decrease in the nitrogen content and/or the formation of an amorphous structure [47,48].

The comparison between the hardness of high-entropy coatings and multilayered coatings is also of interest. In the latter case, hardness improves due to the alternation of nanosized layers of different nitrides [114–126]. Both binary [114–123,193] and multicomponent (including high-entropy) nitrides [72,125,126,193] can be used in multilayer coatings. The highest hardness was observed in multilayer coatings based on (i) multicomponent nitrides (e.g., (TiAlCrY/Zr)/(TiAlCrYN/ZrN)—68 GPa [126]) or (ii) coatings comprising Si-containing nitrides with a nanocomposite structure (see Section 2) (e.g., (Ti,Al)N/(Ti,Si)N—58 GPa [125]). However, it should be noted that the hardness of highentropy and multi-layer coatings is rather similar (Figure 6).

## 4.2. Tribological Properties

Another important property of HEN coatings is high wear resistance. Tribological properties of HEN coatings were discussed in many papers [37,63,76,127–134]. However, the analysis of the obtained results is complicated by the fact that data for the comparison are usually limited to the coatings of one system produced using different deposition parameters [76,129–133] or to coatings without nitrogen [76,132]. Meanwhile, the comparison of wear resistance with those of binary and ternary systems is missing in many articles [76,129–132,134]. Some limitations are also associated with using different schemes and parameters of tribological tests.

In the most systematic study [37], wear resistances of binary TiN, ternary TiAlN and high-entropy (AlCrNbSiTi)N coatings deposited on WC/Co milling inserts were compared. The hardness levels of the TiN, TiAlN and (AlCrNbSiTi)N coatings were 20, 30 and 36 GPa, respectively. In dry machining of SKD11 (260 HV) (Figure 7a) and 304 stainless steel (190 HV) (Figure 7b), the wear of the inserts coated with (AlCrNbSiTi)N was found to be minimal. Cutting of the 304 steel under severe conditions (cutting speed of 160 m/min) (Figure 7c) also suggests less pronounced wear depth of the HEN-coated milling inserts in comparison with those coated by TiN and TiAlN (by 23% and 25%, respectively) [37]. Under such conditions, the temperature at the contact point between the workpiece and tool increased considerably. The improved wear resistance of (AlCrNbSiTi)N coatings was ascribed to both higher hardness and better thermal stability and oxidation resistance.

Apparently, wear resistance of HEN coatings is dependent on hardness, which, in turn, depend on composition, structure and deposition parameters, as was discussed in the previous section. The dependence of the wear resistance and hardness of nitride (TiZrNbTaFe)N coatings obtained at different  $N_2/Ar$  ratios on hardness is shown in Figure 8 [76]. The coating with the nitrogen content of 17 at.% had an amorphous structure, similar to the TiZrNbTaFe metallic coating deposited without nitrogen. At the nitrogen content of 32–39 at.%, a single-phase fcc crystal structure was formed. The hardness of the coatings varied from 22 to 36 GPa. The wear rate of the coatings was inversely proportional to hardness, which is fully consistent with the Archard law [135].

The effect of magnetron sputtering parameters (such as the  $N_2/Ar$  ratio or bias potential on the substrate) on the wear resistance of high-entropy (CrAlTiNbV)N coatings was comprehensively studied in [130,131]. An increase in the nitrogen flow and the bias potential resulted in the formation of a finer and denser structure with higher hardness and a better wear resistance. Meanwhile, as the nitrogen flow rate increased to a maximum value of 48 sccm [130], the hardness and wear resistance of coatings dropped sharply due to the crystallite growth.

Metals **2022**, 12, 847

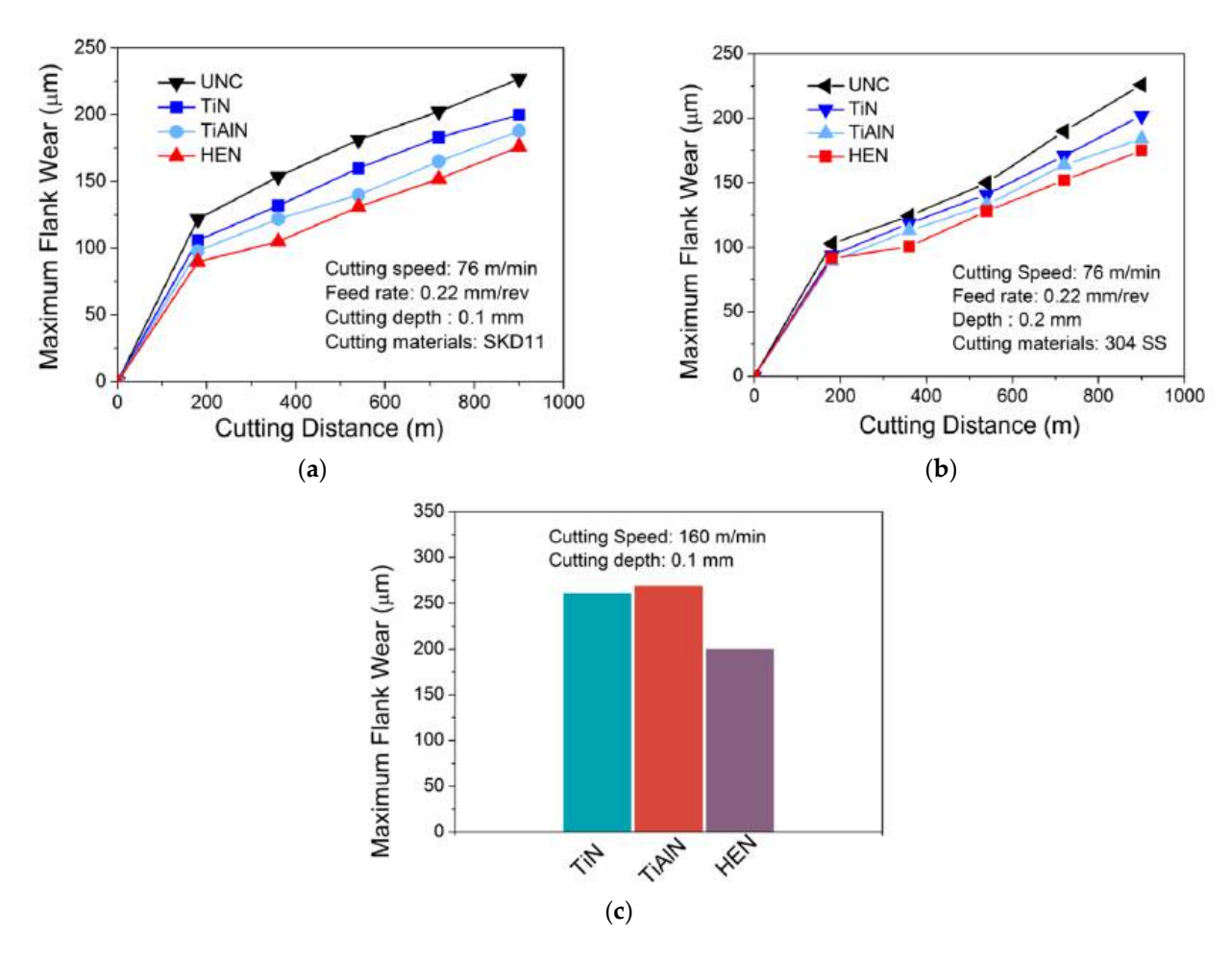


**Figure 7.** Maximum flank wear depths of uncoated TiN-, TiAlN- and  $(Al_{0.34}Cr_{0.22}Nb_{0.11}Si_{0.11}Ti_{0.22})_{50}N_{50}$ -coated inserts milling against (a) SKD11 steel and (b) 304 stainless steel as a function of cutting distance in the interrupted dry face milling test; (c) the comparison of maximum flank wear among TiN-, TiAlN- and HEN-coated inserts after continuous dry milling tests against 304 stainless steel for a cutting distance of 900 m. Reproduced from [37].

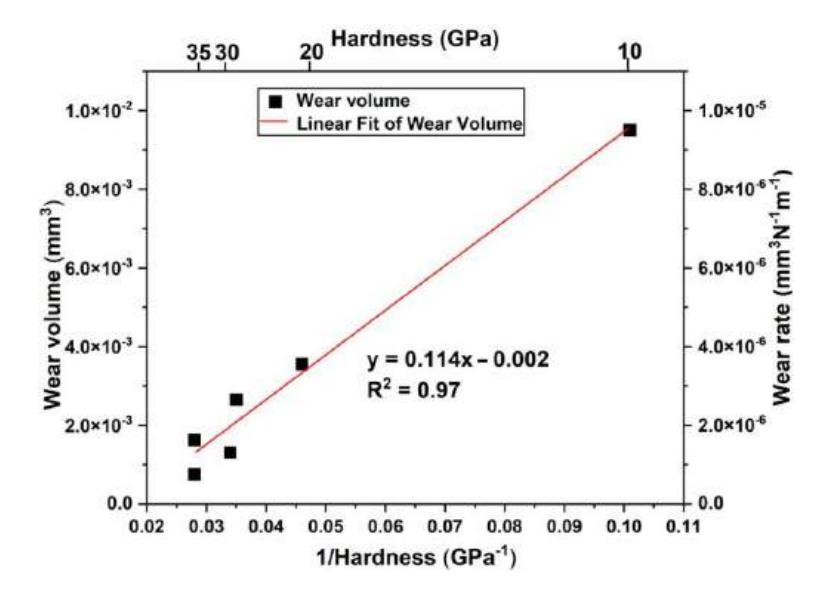


**Figure 8.** Dependence of wear on hardness of (TiZrNbTaFe)N coatings. Archard's law experimental results. Reprinted with permission from ref. [76]. Copyright 2021 Elsevier.

Metals **2022**, 12, 847 14 of 23

In order to improve the tribological properties of HEN coatings, some elements (e.g., Mo, V or W) can be added, by analogy with conventional multicomponent nitrides, to reduce the friction coefficient and wear rate [136]. The addition of these elements results in the formation of the Magneli phase [137], a layered crystal structure of which reduces the friction coefficient [138,139]. For example, the formation of MoO<sub>3</sub> in coatings containing molybdenum at temperatures above 600 °C yields a self-lubricating surface [140,141]. In [129], the effect of Mo on (AlCrTaTiZr)N coatings was examined. The (AlCrMoTaTiZr)N coatings had an excellent wear resistance of  $2.9 \times 10^{-6} \text{ mm}^3/\text{N} \times \text{m}$  as compared with the Mo-free (AlCrTaTiZr)N coatings (wear rate was in the range of 3.7–6.5  $10^{-6}$  mm<sup>3</sup>/N × m) [129]. Lower wear and friction coefficient in this case was associated with the formation of a lubricating layer during friction due to Mo addition. Tribological properties of Mo-containing (AlCrNbSiTiMo)N coatings were studied in [142] at room and elevated temperatures. During tests at room temperature and 700 °C, the friction coefficients of the coatings were 0.68 and 0.48, respectively. In addition, the value of the friction coefficient gradually decreased during wear at 700 °C, thereby suggesting the lubricating effect of molybdenum oxides found on the surface using X-ray photoelectron spectroscopy.

The wear resistance of coatings also depends on their oxidation resistance. At high friction rates, the temperature in the contact zone can reach 1000 °C due to local heating. As a result, deterioration in the wear resistance of the coatings can happen because of (among some other possible reasons) the onset of the oxidation process. Tribological tests of (CrAlNbSiV)N coatings were performed using a "ball-to-disk" scheme with a 6 mm Al<sub>2</sub>O<sub>3</sub> counterbody at room temperature and at 600 °C [128]. The wear rate was  $2 \times 10^{-6}$  mm<sup>3</sup> N<sup>-1</sup> m<sup>-1</sup>, i.e., much lower than that of the (AlCrTaTiZr)N [133], (AlCrMoTaTiZr)N [129] and (TiZrNbHfTa)N [143] coatings (Table 3). The relatively low wear rate was ascribed to a high value of the  $H^3/E^2$  (hardness to elastic modulus) ratio of about 0.52 at the hardness of 35 GPa. At 600 °C, more pronounced oxidation (the oxygen concentration ~50 at.%) was observed in the friction zone in comparison with the area next to the wear trace (7–8 at.%). This difference can be associated with (i) some additional increase in temperature in the friction zone, (ii) an increase in the depth of oxygen penetration due to the formation of cracks and (iii) depletion of aluminum in the coating due to wear and thinning of the surface oxide layer. Although the oxide layer reduced the friction coefficient from 0.88 to 0.63, the wear rate slightly increased (up to  $5.4 \times 10^{-6}$  mm<sup>3</sup> N<sup>-1</sup> × m<sup>-1</sup>). However, oxidation does not lead to complete degradation of the coating, since nitrogen was still found inside the wear scars that indirectly suggests good oxidation resistance. It is also important to note that at 600 °C, this high-entropy coating had a lower wear rate than that of the binary nitride CrN [144], ternary nitrides CrAlN [145] and TiAlN [146] and quaternary nitrides CrAlSiN [145] and TiAlSiN [147] under similar test conditions (Table 3). Thus, the good wear resistance of this system at elevated temperatures is most likely associated with the presence of Al, Cr and Si that improves the oxidation resistance due to the formation of protective oxide layers [34]. It was shown in [148–151] that the addition of the above elements to ternary and quaternary nitrides improves their resistance to oxidation. Thus, oxidation resistance of high-entropy coating (TiVCrZrHf)N [152], which does not contain Al and Si, is close to that of a simple binary nitride TiN [153]. Annealing in air for two hours resulted in the onset of oxidation of the coating at 400 °C and in almost complete oxidation at 600 °C. At the same time, the (AlCrNbSiTi)N coating [34], containing the above elements, remains resistant to oxidation even at 1300 °C. Thus, good wear resistance of high-entropy coatings is associated with high hardness, high H<sup>3</sup>/E<sup>2</sup> ratios, lower friction coefficients at elevated temperatures and good oxidation resistance. Coatings containing both elements that reduce the friction coefficient (e.g., Mo, V) and those which improve the oxidation resistance (e.g., Al, Si) are the most promising for tribological applications. For example, the (AlCrNbSiTiMo)N coating [142] combines a low wear rate and a low friction coefficient at elevated temperatures (Table 4), approaching the corresponding values of binary MoN [165].

Metals 2022, 12, 847 15 of 23

System of Coating	Counterbody	Testing Temperature, °C	Thickness of Coating, µm	Coefficient of Friction	Wear Rate, $\times 10^{-6}~mm^3~N^{-1}\times m^{-1}$	References
TiN	sapphire, 6 mm ball	RT	2.1	0.84	4.4	[143]
CrN	$Al_2O_3$ , 6 mm ball	600	3.3	0.46	12	[144]
MoN	$Al_2O_3$ , 6 mm ball	RT 600	1.65	$0.4 \\ 0.4$	16 70	[165]
TiAlN	SiC, 6 mm ball	600	5.86	0.5	10	[146]
CrAlN	Al <sub>2</sub> O <sub>3</sub> , 6 mm ball	RT 600	2.2	0.5 completely worn	0.6 completely worn	[145]
CrAlSiN	Al <sub>2</sub> O <sub>3</sub> , 6 mm ball	RT 600	2.1	0.6 completely worn	0.25 completely worn	[145]
TiAlSiN	$Al_2O_3$ , 6 mm ball	600	1.8	0.6	10	[147]
(CrAlNbSiV)N	Al <sub>2</sub> O <sub>3</sub> , 6 mm ball	RT 600	~0.8	0.88 0.63	2 5.4	
(AlCrTaTiZr)N	100Cr6 (AISI 52100) steel, 6.35 mm ball	RT	1.0-1.3	0.76	3.65	[133]
(AlCrMoTaTiZr)N	100Cr6 (AISI 52100) steel, 6.35 mm ball	RT	1.2–1.5	0.74	2.8	[129]
(AlCrNbSiTiMo)N	$Al_2O_3$ , 6 mm ball	RT 700	~1	0.68 0.48	- 1.2	[142]
(TiZrNbHfTa)N	sapphire, 6 mm ball	RT	2.0	0.96	2.9	[143]
(TiZrNbTaFe)N	WC-6 wt% Co, 6 mm ball	RT	0.9	0.69	2.65	[76]

**Table 4.** Tribological properties of binary, ternary, quaternary and high-entropy nitride coatings.

#### 5. Conclusions

High-entropy nitride coatings have several highly attractive features: high stability of a single-phase structure, high hardness up to 60 GPa, and excellent oxidation resistance up to 1300 °C. These features are often related to high mixing entropy, yet these claims are mostly not supported with solid evidence. The performed analysis has revealed that the coatings composed of groups IV-V metals are prone to the formation of the NaCl-type MeN nitrides with stable solid solution structure. The stability of such coatings at high temperatures is ultimately limited by the temperatures at which nitrogen evaporates. The addition of Al or Si, which usually form hcp covalent nitrides, destabilizes the solid solution and leads to the formation of amorphous and/or hcp phases. The microstructure and hardness of HEN coatings depend mainly on parameters of the deposition processes. Under similar deposition parameters, an increase in the number of components results in an increase in hardness of the coatings. Improved tribological properties can be achieved by adding elements (Mo or W) that reduce friction coefficients. The addition of Al and Si increases oxidation resistance due to the formation of protective oxide layers. Thus, comprehensive properties profiles can be achieved by tailoring the composition of HEN coatings. The most promising industrial application of HEN coatings is the protection of parts operating under friction and erosive wear at high temperatures. However, there is currently a lack of systematic studies on the effect of chemical composition on the properties of the coatings produced using similar deposition conditions. This crucial disadvantage must be overcome to produce the all-around alloying concept. In addition, theoretical studies on various thermodynamic aspects of behavior of HEN coatings are required.

Author Contributions: V.N. performed the data collection, analysis and interpretation; N.S. and S.Z. critically revised the manuscript; G.S. conceptualized the work and provided the resources. All authors have read and agreed to the published version of the manuscript.

Funding: The authors gratefully acknowledge the financial support of the Russian Science Foundation Grant no. 19-79-30066 (https://rscf.ru/project/19-79-30066; accessed date 3 May 2022). The work was carried out using the equipment of the Joint Research Center of Belgorod State National Research University "Technology and Materials" with financial support from the Ministry of Science and Higher Education of the Russian Federation within the framework of agreement No. 075-15-2021-690 (unique identifier for the project: RF—2296.61321X0030).

Acknowledgments: The authors gratefully acknowledge the financial support from the Russian Science Foundation Grant no. 19-79-30066 (https://rscf.ru/project/19-79-30066; accessed date 3 May 2022). The work was carried out using the equipment of the Joint Research Center of Belgorod State National Research University "Technology and Materials".

Metals **2022**, 12, 847 16 of 23

#### **Conflicts of Interest:** The authors declare no conflict of interest.

#### References

- 1. Bobzin, K. High-performance coatings for cutting tools. CIRP J. Manuf. Sci. Technol. 2017, 18, 1–9. [CrossRef]
- Feuerstein, A.; Kleyman, A. Ti–N multilayer systems for compressor airfoil sand erosion protection. Surf. Coat. Technol. 2009, 204, 1092–1096. [CrossRef]
- 3. Holleck, H. Material selection for hard coatings. J. Vac. Sci. Technol. A 1986, 4, 2661–2669. [CrossRef]
- 4. Steyer, P.; Mege, A.; Pech, D.; Mendibide, C.; Fontaine, J.; Pierson, J.-F.; Esnouf, C.; Goudeau, P. Influence of the nanostructuration of PVD hard TiN-based films on the durability of coated steel. *Surf. Coat. Technol.* **2008**, 202, 2268–2277. [CrossRef]
- 5. Deng, J.; Liu, J.; Zhao, J.; Song, W. Wear mechanisms of PVD ZrN coated tools in machining. *Int. J. Refract. Met. Hard Mater.* **2008**, 26, 164–172. [CrossRef]
- 6. Chim, Y.C.; Ding, X.Z.; Zeng, X.T.; Zhang, S. Oxidation resistance of TiN, CrN, TiAlN and CrAlN coatings deposited by lateral rotating cathode arc. *Thin Solid Films* **2009**, *517*, 4845–4849. [CrossRef]
- 7. Sproul, W.D.; Graham, M.E.; Wong, M.-S.; Rudnik, P.J. Reactive unbalanced magnetron sputtering of the nitrides of Ti, Zr, Hf, Cr, Mo, Ti-Al, Ti-Zr and Ti-Al-V. Surf. Coat. Technol. 1993, 61, 139–143. [CrossRef]
- 8. Panjan, P.; Navinšek, B.; Cvelbar, A.; Zalar, A.; Milošev, I. Oxidation of TiN, ZrN, TiZrN, CrN, TiCrN and TiN/CrN multilayer hard coatings reactively sputtered at low temperature. *Thin Solid Films* **1996**, *281*–*282*, 298–301. [CrossRef]
- 9. Jehn, H.A. Multicomponent and multiphase hard coatings for tribological applications. *Surf. Coat. Technol.* **2000**, *131*, 433–440. [CrossRef]
- 10. Hörling, A.; Hultman, L.; Odén, M.; Sjölén, J.; Karlsson, L. Mechanical properties and machining performance of Ti1–xAlxN-coated cutting tools. *Surf. Coat. Technol.* **2005**, *191*, 384–392. [CrossRef]
- 11. Cheng, Y.H.; Browne, T.; Heckerman, B.; Meletis, E.I. Mechanical and tribological properties of nanocomposite TiSiN coatings. *Surf. Coat. Technol.* **2010**, 204, 2123–2129. [CrossRef]
- 12. Veprek, S.; Veprek-Heijman, M.J.G. Industrial applications of superhard nanocomposite coatings. *Surf. Coat. Technol.* **2008**, 202, 5063–5073. [CrossRef]
- 13. Barshilia, H.C.; Acharya, S.; Ghosh, M.; Suresh, T.N.; Rajam, K.S.; Konchady, M.S.; Pai, D.M.; Sankar, J. Performance evaluation of TiAlCrYN nanocomposite coatings deposited using four-cathode reactive unbalanced pulsed direct current magnetron sputtering system. *Vacuum* **2010**, *85*, 411–420. [CrossRef]
- 14. Shen, L.; Zhao, J.; Zhang, Y.-Q.; Quan, G.-Z. Performance evaluation of titanium-based metal nitride coatings and die lifetime prediction in a cold extrusion process. *High Temp. Mater. Process.* **2021**, *40*, 108–120. [CrossRef]
- 15. Hasegawa, H.; Kimura, A.; Suzuki, T. Microhardness and structural analysis of (Ti,Al)N, (Ti,Cr)N, (Ti,Zr)N and (Ti,V)N films. *J. Vac. Sci. Technol. A* **2000**, *18*, 1038–1040. [CrossRef]
- 16. Lin, J.; Mishra, B.; Moore, J.J.; Sproul, W.D. A study of the oxidation behavior of CrN and CrAlN thin films in air using DSC and TGA analyses. *Surf. Coat. Technol.* **2008**, 202, 3272–3283. [CrossRef]
- 17. Yoo, Y.H.; Le, D.P.; Kim, J.G.; Kim, S.K.; Vinh, P.V. Corrosion behavior of TiN, TiAlN, TiAlSiN thin films deposited on tool steel in the 3.5 wt.% NaCl solution. *Thin Solid Films* **2008**, *516*, 3544–3548. [CrossRef]
- 18. Hsu, T.-W.; Greczynski, G.; Boyd, R.; Kolozsvári, S.; Polcik, P.; Bolz, S.; Bakhit, B.; Odén, M. Influence of Si content on phase stability and mechanical properties of TiAlSiN films grown by AlSi-HiPIMS/Ti-DCMS co-sputtering. *Surf. Coat. Technol.* **2021**, 427, 127661. [CrossRef]
- 19. Moser, M.; Mayrhofer, P.H. Yttrium-induced structural changes in sputtered Ti<sub>1-x</sub>Al<sub>x</sub>N thin films. *Scr. Mater.* **2007**, *57*, 357–360. [CrossRef]
- 20. Yeh, J.-W.; Chen, S.-K.; Lin, S.-J.; Gan, J.-Y.; Chin, T.-S.; Shun, T.-T.; Tsau, C.-H.; Chang, S.-Y. Nanostructured High-Entropy Alloys with Multiple Principal Elements: Novel Alloy Design Concepts and Outcomes. *Adv. Eng. Mater.* **2004**, *6*, 299–303. [CrossRef]
- 21. Li, A.; Zhang, X. Thermodynamic analysis of the simple microstructure of AlCrFeNiCu high-entropy alloy with multi-principal elements. *Acta Metall. Sin.* **2009**, 22, 219–224. [CrossRef]
- 22. Tsai, M.-H.; Yeh, J.-W. High-Entropy Alloys: A Critical Review. Mater. Res. Lett. 2014, 2, 107–123. [CrossRef]
- 23. Zhang, Y.; Zuo, T.T.; Tang, Z.; Gao, M.C.; Dahmen, K.A.; Liaw, P.K.; Lu, Z.P. Microstructures and properties of high-entropy alloys. *Prog. Mater. Sci.* **2014**, *61*, 1–93. [CrossRef]
- 24. Ye, Y.F.; Wang, Q.; Lu, J.; Liu, C.T.; Yang, Y. High-entropy alloy: Challenges and prospects. *Mater. Today* **2016**, *19*, 349–362. [CrossRef]
- 25. George, E.P.; Raabe, D.; Ritchie, R.O. High-entropy alloys. Nat. Rev. Mater. 2019, 4, 515–534. [CrossRef]
- 26. Li, W.; Liu, P.; Liaw, P.K. Microstructures and properties of high-entropy alloy films and coatings: A review. *Mater. Res. Lett.* **2018**, 6, 199–229. [CrossRef]
- 27. Pogrebnjak, A.D.; Bagdasaryan, A.A.; Yakushchenko, I.V.; Beresnev, V.M. The structure and properties of high-entropy alloys and nitride coatings based on them. *Russ. Chem. Rev.* **2014**, *83*, 1027–1061. [CrossRef]
- 28. Li, J.; Huang, Y.; Meng, X.; Xie, Y. A Review on High Entropy Alloys Coatings: Fabrication Processes and Property Assessment. *Adv. Eng. Mater.* **2019**, *21*, 1900343. [CrossRef]
- 29. Lewin, E. Multi-component and high-entropy nitride coatings—A promising field in need of a novel approach. *J. Appl. Phys.* **2020**, 127, 160901. [CrossRef]

Metals **2022**, 12, 847 17 of 23

30. Pogrebnjak, A.D. Hard and superhard nanostructured and nanocomposite coatings. In *Nanomaterials-Based Coatings*; Tri, P.N., Rtimi, S., Plamondon, C.M.O., Eds.; Elsevier: Amsterdam, The Netherlands, 2019; pp. 237–337.

- 31. Yeh, J.-W.; Lin, S.-J.; Tsai, M.-H.; Chang, S.-Y. High-entropy coatings. In *High-Entropy Alloys*; Gao, M., Yeh, J.W., Liaw, P., Zhang, Y., Eds.; Springer: Cham, Switzerland, 2016; pp. 469–491.
- 32. Murty, B.S.; Yeh, J.W.; Ranganathan, S.; Bhattacharjee, P.P. High-entropy alloy coatings. In *High-Entropy Alloys*; Murty, B.S., Yeh, J.W., Ranganathan, S., Bhattacharjee, P.P., Eds.; Elsevier: Amsterdam, The Netherlands, 2019; pp. 177–193.
- 33. Ali Alvi, S.; Zhang, H.; Akhtar, F. High-entropy ceramics. In *Engineering Steels and High Entropy-Alloys*; Sharma, A., Duriagina, Z., Kumar, S., Eds.; IntechOpen: London, UK, 2020.
- 34. Shen, W.J.; Tsai, M.H.; Tsai, K.Y.; Juan, C.C.; Tsai, C.W.; Yeh, J.W.; Chang, Y.S. Superior Oxidation Resistance of (Al<sub>0.34</sub>Cr<sub>0.22</sub>Nb<sub>0.11</sub>Si<sub>0.11</sub>Ti<sub>0.22</sub>)<sub>50</sub>N<sub>50</sub>High-Entropy Nitride. *J. Electrochem. Soc.* **2013**, *160*, C531–C535. [CrossRef]
- 35. Huang, P.-K.; Yeh, J.-W. Effects of substrate temperature and post-annealing on microstructure and properties of (AlCrNbSiTiV)N coatings. *Thin Solid Films* **2009**, *518*, 180–184. [CrossRef]
- 36. Firstov, S.A.; Gorban, V.F.; Danilenko, N.I.; Karpets, M.V.; Andreev, A.A.; Makarenko, E.S. Thermal Stability of Superhard Nitride Coatings from High-Entropy Multicomponent Ti–V–Zr–Nb–Hf Alloy. *Powder Metall. Met. Ceram.* **2014**, *52*, 560–566. [CrossRef]
- 37. Shen, W.-J.; Tsai, M.-H.; Yeh, J.-W. Machining Performance of Sputter-Deposited (Al<sub>0.34</sub>Cr<sub>0.22</sub>Nb<sub>0.11</sub>Si<sub>0.11</sub>Ti<sub>0.22</sub>)<sub>50</sub>N<sub>50</sub>High-Entropy Nitride Coatings. *Coatings* **2015**, *5*, 312–325. [CrossRef]
- 38. Muñoz, A.; González, J.; Restrepo, J.; Cano, O.M.; Sequeda, F. Tribology of ZRN, CRN and TIALN thin films deposited by reactive magnetron sputtering. *Dyna* **2013**, *80*, 95–100.
- 39. Boxman, R.L.; Zhitomirsky, V.N.; Grimberg, I.; Rapoport, L.; Goldsmith, S.; Weiss, B.Z. Structure and hardness of vacuum arc deposited multi-component nitride coatings of Ti, Zr and Nb. Surf. Coat. Technol. 2000, 125, 257–262. [CrossRef]
- 40. Tabakov, V.P.; Vereschaka, A.S.; Vereschaka, A.A. Multilayer composition coatings for cutting tools: Formation and performance properties. *Mech. Ind.* **2017**, *18*, 706. [CrossRef]
- 41. Huang, M.; Chen, Z.; Wang, M.; Li, Y.; Wang, Y. Microstructure and properties of TiCrN coatings by arc ion plating. *Surf. Eng.* **2016**, *32*, 284–288. [CrossRef]
- 42. Yazdi, M.A.P.; Lomello, F.; Wang, J.; Sanchette, F.; Dong, Z.; White, T.; Wouters, Y.; Schuster, F.; Billard, A. Properties of TiSiN coatings deposited by hybrid HiPIMS and pulsed-DC magnetron co-sputtering. *Vacuum* **2014**, *109*, 43–51. [CrossRef]
- 43. Zhu, P.; Ge, F.; Li, S.; Xue, Q.; Huang, F. Microstructure, chemical states, and mechanical properties of magnetron co-sputtered V1—xAlxN coatings. *Surf. Coat. Technol.* **2013**, 232, 311–318. [CrossRef]
- 44. Johansson, K.; Riekehr, L.; Fritze, S.; Lewin, E. Multicomponent Hf-Nb-Ti-V-Zr nitride coatings by reactive magnetron sputter deposition. *Surf. Coat. Technol.* **2018**, 349, 529–539. [CrossRef]
- 45. Von Fieandt, K.; Paschalidou, E.-M.; Srinath, A.; Soucek, P.; Riekehr, L.; Nyholm, L.; Lewin, E. Multi-component (Al,Cr,Nb,Y,Zr)N thin films by reactive magnetron sputter deposition for increased hardness and corrosion resistance. *Thin Solid Films* **2020**, 693, 137685. [CrossRef]
- 46. Chang, Z.-C.; Liang, S.-C.; Han, S.; Chen, Y.-K.; Shieu, F.-S. Characteristics of TiVCrAlZr multi-element nitride films prepared by reactive sputtering. *Nucl. Instrum. Methods Phys. Res. Sect. B* **2010**, 268, 2504–2509. [CrossRef]
- 47. Feng, X.; Tang, G.; Ma, X.; Sun, M.; Wang, L. Characteristics of multi-element (ZrTaNbTiW)N films prepared by magnetron sputtering and plasma based ion implantation. *Nucl. Instrum. Methods Phys. Res. Sect. B* **2013**, 301, 29–35. [CrossRef]
- 48. Sheng, W.; Yang, X.; Wang, C.; Zhang, Y. Nano-Crystallization of High-Entropy Amorphous NbTiAlSiWxNy Films Prepared by Magnetron Sputtering. *Entropy* **2016**, *18*, 226. [CrossRef]
- 49. Sobol, O.; Andreev, A.A.; Gorban, V.; Postelnyk, H.O.; Stolbovoy, V.A.; Zvyagolsky, A.V.; Dolomanov, A.V.; Kraievska, Z.V. The use of negative bias potential for structural engineering of vacuum-arc nitride coatings based on high-entropy alloys. *Probl. At. Sci. Technol.* **2019**, *120*, 127–135. [CrossRef]
- 50. Liang, S.-C.; Tsai, D.-C.; Chang, Z.-C.; Sung, H.-S.; Lin, Y.-C.; Yeh, Y.-J.; Deng, M.-J.; Shieu, F.-S. Structural and mechanical properties of multi-element (TiVCrZrHf)N coatings by reactive magnetron sputtering. *Appl. Surf. Sci.* **2011**, 258, 399–403. [CrossRef]
- 51. Tsai, D.-C.; Huang, Y.-L.; Lin, S.-R.; Liang, S.-C.; Shieu, F.-S. Effect of nitrogen flow ratios on the structure and mechanical properties of (TiVCrZrY)N coatings prepared by reactive magnetron sputtering. *Appl. Surf. Sci.* **2010**, 257, 1361–1367. [CrossRef]
- 52. Chang, H.-W.; Huang, P.-K.; Davison, A.; Yeh, J.-W.; Tsau, C.-H.; Yang, C.-C. Nitride films deposited from an equimolar Al–Cr–Mo–Si–Ti alloy target by reactive direct current magnetron sputtering. *Thin Solid Films* **2008**, *516*, 6402–6408. [CrossRef]
- 53. Yan, X.H.; Li, J.S.; Zhang, W.R.; Zhang, Y. A brief review of high-entropy films. Mater. Chem. Phys. 2018, 210, 12–19. [CrossRef]
- 54. Dolique, V.; Thomann, A.-L.; Brault, P. High-Entropy Alloys Deposited by Magnetron Sputtering. *IEEE Trans. Plasma Sci.* **2011**, 39, 2478–2479. [CrossRef]
- 55. Xu, Y.; Li, G.; Xia, Y. Synthesis and characterization of super-hard AlCrTiVZr high-entropy alloy nitride films deposited by HiPIMS. *Appl. Surf. Sci.* **2020**, 523, 146529. [CrossRef]
- 56. Li, X.; Zheng, Z.; Dou, D.; Li, J. Microstructure and Properties of Coating of FeAlCuCrCoMn High Entropy Alloy Deposited by Direct Current Magnetron Sputtering. *Mater. Res.* **2016**, *19*, 802–806. [CrossRef]
- 57. Dedoncker, R.; Djemia, P.; Radnóczi, G.; Tétard, F.; Belliard, L.; Abadias, G.; Martin, N.; Depla, D. Reactive sputter deposition of CoCrCuFeNi in nitrogen/argon mixtures. *J. Alloys Compd.* **2018**, *769*, 881–888. [CrossRef]

Metals **2022**, 12, 847 18 of 23

58. Ren, B.; Yan, S.Q.; Zhao, R.F.; Liu, Z.X. Structure and properties of (AlCrMoNiTi)Nx and (AlCrMoZrTi)Nx films by reactive RF sputtering. *Surf. Coat. Technol.* **2013**, 235, 764–772. [CrossRef]

- 59. Alvi, S.; Jarzabek, D.M.; Kohan, M.G.; Hedman, D.; Jenczyk, P.; Natile, M.M.; Vomiero, A.; Akhtar, F. Synthesis and Mechanical Characterization of a CuMoTaWV High-Entropy Film by Magnetron Sputtering. *ACS Appl. Mater. Interfaces* **2020**, *12*, 21070–21079. [CrossRef]
- 60. Chen, T.K.; Shun, T.T.; Yeh, J.W.; Wong, M.S. Nanostructured nitride films of multi-element high-entropy alloys by reactive DC sputtering. *Surf. Coat. Technol.* **2004**, *188–189*, 193–200. [CrossRef]
- 61. Liu, L.; Zhu, J.B.; Hou, C.; Li, J.C.; Jiang, Q. Dense and smooth amorphous films of multicomponent FeCoNiCuVZrAl high-entropy alloy deposited by direct current magnetron sputtering. *Mater. Des.* **2013**, *46*, 675–679. [CrossRef]
- 62. Sha, C.; Zhou, Z.; Xie, Z.; Munroe, P. FeMnNiCoCr-based high entropy alloy coatings: Effect of nitrogen additions on microstructural development, mechanical properties and tribological performance. *Appl. Surf. Sci.* **2020**, *507*, 145101. [CrossRef]
- 63. Pogrebnjak, A.D.; Yakushchenko, I.V.; Bagdasaryan, A.A.; Bondar, O.V.; Krause-Rehberg, R.; Abadias, G.; Chartier, P.; Oyoshi, K.; Takeda, Y.; Beresnev, V.M.; et al. Microstructure, physical and chemical properties of nanostructured (Ti–Hf–Zr–V–Nb)N coatings under different deposition conditions. *Mater. Chem. Phys.* **2014**, *147*, 1079–1091. [CrossRef]
- 64. Beresnev, V.M.; Sobol, O.V.; Andreev, A.A.; Gorban, V.F.; Klimenko, S.A.; Litovchenko, S.V.; Kovteba, D.V.; Meilekhov, A.A.; Postel'nik, A.A.; Nemchenko, U.S.; et al. Formation of Superhard State of the TiZrHfNbTaYN Vacuum–Arc High-Entropy Coating. *J. Superhard Mater.* 2018, 40, 102–109. [CrossRef]
- 65. Liang, S.-C.; Chang, Z.-C.; Tsai, D.-C.; Lin, Y.-C.; Sung, H.-S.; Deng, M.-J.; Shieu, F.S. Effects of substrate temperature on the structure and mechanical properties of (TiVCrZrHf)N coatings. *Appl. Surf. Sci.* **2011**, 257, 7709–7713. [CrossRef]
- 66. Zhao, Y.; Chen, S.; Chen, Y.; Wu, S.; Xie, W.; Yan, W.; Wang, S.; Liao, B.; Zhang, S. Super-hard and anti-corrosion (AlCrMoSiTi)Nx high entropy nitride coatings by multi-arc cathodic vacuum magnetic filtration deposition. *Vacuum* **2022**, *195*, 110685. [CrossRef]
- 67. Yalamanchili, K.; Wang, F.; Schramm, I.C.; Andersson, J.M.; Jöesaar, M.P.J.; Tasnádi, F.; Mücklich, F.; Ghafoor, N.; Odén, M. Exploring the high entropy alloy concept in (AlTiVNbCr)N. *Thin Solid Films* **2017**, *636*, 346–352. [CrossRef]
- 68. Yu, W.; Li, W.; Liu, P.; Zhang, K.; Ma, F.; Chen, X.; Feng, R.; Liaw, P.K. Silicon-content-dependent microstructures and mechanical behavior of (AlCrTiZrMo)-Six-N high-entropy alloy nitride films. *Mater. Des.* **2021**, 203, 109553. [CrossRef]
- 69. Kirnbauer, A.; Kretschmer, A.; Koller, C.M.; Wojcik, T.; Paneta, V.; Hans, M.; Schneider, J.M.; Polcik, P.; Mayrhofer, P.H. Mechanical properties and thermal stability of reactively sputtered multi-principal-metal Hf-Ta-Ti-V-Zr nitrides. *Surf. Coat. Technol.* 2020, 389, 125674. [CrossRef]
- 70. Sobol, O. Structure and properties of high-entropy alloys based on refractory metals. *Mater. Today Proc.* **2020**, *30*, 736–741. [CrossRef]
- 71. Pogrebnjak, A.D.; Yakushchenko, I.V.; Abadias, G.; Chartier, P.; Bondar, O.V.; Beresnev, V.M.; Takeda, Y.; Sobol', O.V.; Oyoshi, K.; Andreyev, A.A.; et al. The effect of the deposition parameters of nitrides of high-entropy alloys (TiZrHfVNb)N on their structure, composition, mechanical and tribological properties. *J. Superhard Mater.* 2013, 35, 356–368. [CrossRef]
- 72. Nyemchenko, U.S.; Beresnev, V.M.; Sobol, O.V.; Lytovchenko, S.V.; Stolbovoy, V.A.; Novikov, V.J.; Meylekhov, A.A.; Postelnyk, A.A.; Kovaleva, M.G. Structure and mechanical properties of nitride multilayer systems on the basis of high entropy alloys and transition metals of group VI. *Probl. At. Sci. Technol.* **2016**, *101*, 112–120.
- 73. Wang, J.-J.; Chang, S.-Y.; Ouyang, F.-Y. Effect of substrate bias on the microstructure and properties of (AlCrSiNbZr)Nx high entropy nitride thin film. *Surf. Coat. Technol.* **2020**, *393*, 125796. [CrossRef]
- 74. Tsai, D.-C.; Chang, Z.-C.; Kuo, L.-Y.; Lin, T.-J.; Lin, T.-N.; Shieu, F.-S. Solid solution coating of (TiVCrZrHf)N with unusual structural evolution. *Surf. Coat. Technol.* **2013**, 217, 84–87. [CrossRef]
- 75. Lai, C.-H.; Lin, S.-J.; Yeh, J.-W.; Davison, A. Effect of substrate bias on the structure and properties of multi-element (AlCrTaTiZr)N coatings. *J. Phys. D Appl. Phys.* **2006**, 39, 4628–4633. [CrossRef]
- 76. Bachani, S.K.; Wang, C.-J.; Lou, B.-S.; Chang, L.-C.; Lee, J.-W. Fabrication of TiZrNbTaFeN high-entropy alloys coatings by HiPIMS: Effect of nitrogen flow rate on the microstructural development, mechanical and tribological performance, electrical properties and corrosion characteristics. *J. Alloys Compd.* **2021**, *873*, 159605. [CrossRef]
- 77. Rickerby, D.S. Internal stress and adherence of titanium nitride coatings. J. Vac. Sci. Technol. A 1986, 4, 2809–2814. [CrossRef]
- 78. Chen, L.; Chang, K.K.; Du, Y.; Li, J.R.; Wu, M.J. A comparative research on magnetron sputtering and arc evaporation deposition of Ti–Al–N coatings. *Thin Solid Films* **2011**, *519*, 3762–3767. [CrossRef]
- 79. Pierson, H.O. Interstitial nitrides. In *Handbook of Refractory Carbides and Nitrides*; Pierson, H.O., Ed.; William Andrew Publishing: Norwich, NY, USA, 1996; pp. 163–180.
- 80. Pierson, H.O. Covalent nitrides. In *Handbook of Refractory Carbides and Nitrides*; Pierson, H.O., Ed.; William Andrew Publishing: Norwich, NY, USA, 1996; pp. 209–222.
- 81. Matenoglou, G.M.; Koutsokeras, L.E.; Lekka, C.E.; Abadias, G.; Kosmidis, C.; Evangelakis, G.A.; Patsalas, P. Structure, stability and bonding of ternary transition metal nitrides. *Surf. Coat. Technol.* **2009**, 204, 911–914. [CrossRef]
- 82. Abadias, G.; Djemia, P.; Belliard, L. Alloying effects on the structure and elastic properties of hard coatings based on ternary transition metal (M = Ti, Zr or Ta) nitrides. *Surf. Coat. Technol.* **2014**, 257, 129–137. [CrossRef]
- 83. Lengauer, W. Nitrides: Transition metal solid-state chemistry. In *Encyclopedia of Inorganic and Bioinorganic Chemistry*; John Wiley & Sons: Hoboken, NJ, USA, 2015; pp. 1–24.
- 84. Oses, C.; Toher, C.; Curtarolo, S. High-entropy ceramics. *Nat. Rev. Mater.* **2020**, *5*, 295–309. [CrossRef]

Metals **2022**, 12, 847 19 of 23

85. Ye, Y.F.; Zhang, Y.H.; He, Q.F.; Zhuang, Y.; Wang, S.; Shi, S.Q.; Hu, A.; Fan, J.; Yang, Y. Atomic-scale distorted lattice in chemically disordered equimolar complex alloys. *Acta Mater.* **2018**, *150*, 182–194. [CrossRef]

- 86. Chang, C.-C.; Hsiao, Y.-T.; Chen, Y.-L.; Tsai, C.-Y.; Lee, Y.-J.; Ko, P.-H.; Chang, S.-Y. Lattice distortion or cocktail effect dominates the performance of Tantalum-based high-entropy nitride coatings. *Appl. Surf. Sci.* **2022**, *577*, 151894. [CrossRef]
- 87. Zhao, S. Lattice distortion in high-entropy carbide ceramics from first-principles calculations. *J. Am. Ceram. Soc.* **2021**, 104, 1874–1886. [CrossRef]
- 88. Huang, P.-K.; Yeh, J.-W. Effects of nitrogen content on structure and mechanical properties of multi-element (AlCrNbSiTiV)N coating. *Surf. Coat. Technol.* **2009**, 203, 1891–1896. [CrossRef]
- 89. Chang, Z.-C. Structure and properties of duodenary (TiVCrZrNbMoHfTaWAlSi)N coatings by reactive magnetron sputtering. *Mater. Chem. Phys.* **2018**, 220, 98–110. [CrossRef]
- 90. Huang, P.-K.; Yeh, J.-W. Inhibition of grain coarsening up to 1000 °C in (AlCrNbSiTiV)N superhard coatings. *Scr. Mater.* **2010**, *62*, 105–108. [CrossRef]
- 91. Tsai, M.-H.; Lai, C.-H.; Yeh, J.-W.; Gan, J.-Y. Effects of nitrogen flow ratio on the structure and properties of reactively sputtered (AlMoNbSiTaTiVZr)Nx coatings. *J. Phys. D Appl. Phys.* **2008**, *41*, 235402. [CrossRef]
- 92. Rovere, F.; Music, D.; Ershov, S.; Baben, M.; Fuss, H.-G.; Mayrhofer, P.H.; Schneider, J.M. Experimental and computational study on the phase stability of Al-containing cubic transition metal nitrides. *J. Phys. D Appl. Phys.* **2010**, *43*, 035302. [CrossRef]
- 93. Landolt, H.; Börnstein, R. Physikalisch-chemische Tabellen. Z. Anal. Chem. 1884, 23, 49. [CrossRef]
- 94. Koller, C.M.; Kirnbauer, A.; Rachbauer, R.; Kolozsvári, S.; Mayrhofer, P.H. Thermally-induced phase transformation sequence of arc evaporated Ta–Al–N coatings. *Scr. Mater.* **2016**, *113*, 75–78. [CrossRef]
- 95. Santana, A.E.; Karimi, A.; Derflinger, V.H.; Schütze, A. The role of hcp-AlN on hardness behavior of Ti1–xAlxN nanocomposite during annealing. *Thin Solid Films* **2004**, 469–470, 339–344. [CrossRef]
- 96. Ruiz-Yi, B.; Bunn, J.K.; Stasak, D.; Mehta, A.; Besser, M.; Kramer, M.J.; Takeuchi, I.; Hattrick-Simpers, J. The Different Roles of Entropy and Solubility in High Entropy Alloy Stability. *ACS Comb. Sci.* **2016**, *18*, 596–603. [CrossRef]
- 97. Cheng, K.-H.; Tsai, C.-W.; Lin, S.-J.; Yeh, J.-W. Effects of silicon content on the structure and mechanical properties of (AlCrTaTiZr)–Six–N coatings by reactive RF magnetron sputtering. *J. Phys. D Appl. Phys.* **2011**, *44*, 205405. [CrossRef]
- 98. Tsai, D.-C.; Chang, Z.-C.; Kuo, B.-H.; Chang, S.-Y.; Shieu, F.-S. Effects of silicon content on the structure and properties of (AlCrMoTaTi)N coatings by reactive magnetron sputtering. *J. Alloys Compd.* **2014**, *616*, 646–651. [CrossRef]
- 99. Tsai, D.-C.; Deng, M.-J.; Chang, Z.-C.; Kuo, B.-H.; Chen, E.-C.; Chang, S.-Y.; Shieu, F.-S. Oxidation resistance and characterization of (AlCrMoTaTi)-Si<sub>x</sub>-N coating deposited via magnetron sputtering. *J. Alloys Compd.* **2015**, *647*, 179–188. [CrossRef]
- 100. Kretschmer, A.; Kirnbauer, A.; Moraes, V.; Primetzhofer, D.; Yalamanchili, K.; Rudigier, H.; Mayrhofer, P.H. Improving phase stability, hardness, and oxidation resistance of reactively magnetron sputtered (Al,Cr,Nb,Ta,Ti)N thin films by Si-alloying. *Surf. Coat. Technol.* **2021**, *416*, 127162. [CrossRef]
- 101. Vepřek, S.; Reiprich, S. A concept for the design of novel superhard coatings. Thin Solid Films 1995, 268, 64–71. [CrossRef]
- 102. Sandu, C.S.; Benkahoul, M.; Sanjinés, R.; Lévy, F. Model for the evolution of Nb–Si–N thin films as a function of Si content relating the nanostructure to electrical and mechanical properties. *Surf. Coat. Technol.* **2006**, *201*, 2897–2903. [CrossRef]
- 103. Mercs, D.; Briois, P.; Demange, V.; Lamy, S.; Coddet, C. Influence of the addition of silicon on the structure and properties of chromium nitride coatings deposited by reactive magnetron sputtering assisted by RF plasmas. *Surf. Coat. Technol.* **2007**, 201, 6970–6976. [CrossRef]
- 104. Cheng, Y.H.; Browne, T.; Heckerman, B.; Gannon, P.; Jiang, J.C.; Meletis, E.I.; Bowman, C.; Gorokhovsky, V. Influence of Si content on the structure and internal stress of the nanocomposite TiSiN coatings deposited by large area filtered arc deposition. *J. Phys. D Appl. Phys.* **2009**, 42, 125415. [CrossRef]
- 105. Lin, C.H.; Duh, J.G.; Yeh, J.W. Multi-component nitride coatings derived from Ti–Al–Cr–Si–V target in RF magnetron sputter. *Surf. Coat. Technol.* **2007**, *201*, 6304–6308. [CrossRef]
- 106. Ernst, W.; Neidhardt, J.; Willmann, H.; Sartory, B.; Mayrhofer, P.H.; Mitterer, C. Thermal decomposition routes of CrN hard coatings synthesized by reactive arc evaporation and magnetron sputtering. *Thin Solid Films* **2008**, *517*, 568–574. [CrossRef]
- 107. Pogrebnjak, A.D.; Beresnev, V.M.; Smyrnova, K.V.; Kravchenko, Y.O.; Zukowski, P.V.; Bondarenko, G.G. The influence of nitrogen pressure on the fabrication of the two-phase superhard nanocomposite (TiZrNbAlYCr)N coatings. *Mater. Lett.* **2018**, 211, 316–318. [CrossRef]
- 108. Khan, N.A.; Akhavan, B.; Zhou, C.; Zhou, H.; Chang, L.; Wang, Y.; Liu, Y.; Bilek, M.M.; Liu, Z. High entropy nitride (HEN) thin films of AlCoCrCu<sub>0.5</sub>FeNi deposited by reactive magnetron sputtering. *Surf. Coat. Technol.* **2020**, 402, 126327. [CrossRef]
- 109. Pierson, H.O. The refractory nitrides. In *Handbook of Refractory Carbides and Nitrides*; Pierson, H.O., Ed.; William Andrew Publishing: Norwich, NY, USA, 1996; pp. 156–162.
- 110. Binns, J.; Donnelly, M.-E.; Peña-Alvarez, M.; Wang, M.; Gregoryanz, E.; Hermann, A.; Dalladay-Simpson, P.; Howie, R.T. Direct Reaction between Copper and Nitrogen at High Pressures and Temperatures. *J. Phys. Chem. Lett.* **2019**, *10*, 1109–1114. [CrossRef] [PubMed]
- 111. Rao, S.G.; Shu, R.; Boyd, R.; Greczynski, G.; le Febvrier, A.; Eklund, P. Phase formation and structural evolution of multicomponent (CrFeCo)1-yNy films. *Surf. Coat. Technol.* **2021**, 412, 127059. [CrossRef]

Metals **2022**, 12, 847 20 of 23

112. Wang, Q.; Zhou, F.; Wang, C.; Yuen, M.-F.; Wang, M.; Qian, T.; Matsumoto, M.; Yan, J. Comparison of tribological and electrochemical properties of TiN, CrN, TiAlN and a-C:H coatings in simulated body fluid. *Mater. Chem. Phys.* **2015**, *158*, 74–81. [CrossRef]

- 113. Wang, L.; Zhang, G.; Wood, R.J.K.; Wang, S.C.; Xue, Q. Fabrication of CrAlN nanocomposite films with high hardness and excellent anti-wear performance for gear application. *Surf. Coat. Technol.* **2010**, 204, 3517–3524. [CrossRef]
- 114. Paulitsch, J.; Schenkel, M.; Schintlmeister, A.; Hutter, H.; Mayrhofer, P.H. Low friction CrN/TiN multilayer coatings prepared by a hybrid high power impulse magnetron sputtering/DC magnetron sputtering deposition technique. *Thin Solid Films* **2010**, *518*, 5553–5557. [CrossRef]
- 115. Nordin, M.; Larsson, M.; Hogmark, S. Mechanical and tribological properties of multilayered PVD TiN/CrN, TiN/MoN, TiN/NbN and TiN/TaN coatings on cemented carbide. *Surf. Coat. Technol.* **1998**, *106*, 234–241. [CrossRef]
- 116. Pogrebnjak, A.D.; Eyidi, D.; Abadias, G.; Bondar, O.V.; Beresnev, V.M.; Sobol, O.V. Structure and properties of arc evaporated nanoscale TiN/MoN multilayered systems. *Int. J. Refract. Met. Hard Mater.* **2015**, *48*, 222–228. [CrossRef]
- 117. Zhang, J.J.; Wang, M.X.; Yang, J.; Liu, Q.X.; Li, D.J. Enhancing mechanical and tribological performance of multilayered CrN/ZrN coatings. Surf. Coat. Technol. 2007, 201, 5186–5189. [CrossRef]
- 118. Wang, M.X.; Zhang, J.J.; Yang, J.; Wang, L.Q.; Li, D.J. Influence of Ar/N2 flow ratio on structure and properties of nanoscale ZrN/WN multilayered coatings. *Surf. Coat. Technol.* **2007**, 201, 5472–5476. [CrossRef]
- 119. Ou, Y.X.; Lin, J.; Che, H.L.; Moore, J.J.; Sproul, W.D.; Lei, M.K. Mechanical and tribological properties of CrN/TiN superlattice coatings deposited by a combination of arc-free deep oscillation magnetron sputtering with pulsed dc magnetron sputtering. *Thin Solid Films* **2015**, *594*, 147–155. [CrossRef]
- 120. Barshilia, H.C.; Rajam, K.S. Structure and properties of reactive DC magnetron sputtered TiN/NbN hard superlattices. *Surf. Coat. Technol.* **2004**, *183*, 174–183. [CrossRef]
- 121. Hovsepian, P.E.; Lewis, D.B.; Münz, W.-D. Recent progress in large scale manufacturing of multilayer/superlattice hard coatings. Surf. Coat. Technol. 2000, 133–134, 166–175. [CrossRef]
- 122. Pogrebnjak, A.D.; Beresnev, V.M.; Bondar, O.V.; Postolnyi, B.O.; Zaleski, K.; Coy, E.; Jurga, S.; Lisovenko, M.; Konarski, P.; Rebouta, L.; et al. Superhard CrN/MoN coatings with multilayer architecture. *Mater. Des.* **2018**, *153*, 47–59. [CrossRef]
- 123. Helmersson, U.; Todorova, S.; Barnett, S.A.; Sundgren, J.-E.; Markert, L.C.; Greene, J.E. Growth of single-crystal TiN/VN strained-layer superlattices with extremely high mechanical hardness. *J. Appl. Phys.* **1987**, *62*, 481–484. [CrossRef]
- 124. Wu, W.; Chen, W.; Yang, S.; Lin, Y.; Zhang, S.; Cho, T.-Y.; Lee, G.; Kwon, S.-C. Design of AlCrSiN multilayers and nanocomposite coating for HSS cutting tools. *Appl. Surf. Sci.* **2015**, *351*, 803–810. [CrossRef]
- 125. Carvalho, S.; Ribeiro, E.; Rebouta, L.; Pacaud, J.; Goudeau, P.; Renault, P.O.; Rivière, J.; Tavares, C. PVD grown (Ti,Si,Al)N nanocomposite coatings and (Ti,Al)N/(Ti,Si)N multilayers: Structural and mechanical properties. *Surf. Coat. Technol.* **2003**, 172, 109–116. [CrossRef]
- 126. Novikov, V.Y.; Beresnev, V.M.; Kolesnikov, D.A.; Ivanov, O.N.; Lytovchenko, S.V.; Glukhov, O.V.; Gorokh, D.V.; Kozachenko, A.O.; Krytsyna, E.V.; Sirota, V. Structure and Physicomechanical Properties of Superhard Multicomponent Multilayer (TiAlCrY/Zr)/(TiAlCrYN/ZrN) Coatings with Double Modulation Period of the Structure. *J. Nano Electron. Phys.* 2019, 11, 02027-1–02027-6. [CrossRef]
- 127. Chang, Y.-Y.; Chung, C.-H. Tribological and Mechanical Properties of Multicomponent CrVTiNbZr(N) Coatings. *Coatings* **2021**, 11, 41. [CrossRef]
- 128. Lin, Y.-C.; Hsu, S.-Y.; Song, R.-W.; Lo, W.-L.; Lai, Y.-T.; Tsai, S.-Y.; Duh, J.-G. Improving the hardness of high entropy nitride (Cr<sub>0.35</sub>Al<sub>0.25</sub>Nb<sub>0.12</sub>Si<sub>0.08</sub>V<sub>0.20</sub>)N coatings via tuning substrate temperature and bias for anti-wear applications. *Surf. Coat. Technol.* **2020**, *403*, 126417. [CrossRef]
- 129. Cheng, K.-H.; Lai, C.-H.; Lin, S.-J.; Yeh, J.-W. Structural and mechanical properties of multi-element (AlCrMoTaTiZr)Nx coatings by reactive magnetron sputtering. *Thin Solid Films* **2011**, *519*, 3185–3190. [CrossRef]
- 130. Lu, X.; Zhang, C.; Wang, C.; Cao, X.; Ma, R.; Sui, X.; Hao, J.; Liu, W. Investigation of (CrAlTiNbV)Nx high-entropy nitride coatings via tailoring nitrogen flow rate for anti-wear applications in aviation lubricant. *Appl. Surf. Sci.* **2021**, *557*, 149813. [CrossRef]
- 131. Lu, X.; Zhang, C.; Zhang, X.; Cao, X.; Kang, J.; Sui, X.; Hao, J.; Liu, W. Dependence of mechanical and tribological performance on the microstructure of (CrAlTiNbV)Nx high-entropy nitride coatings in aviation lubricant. *Ceram. Int.* **2021**, *47*, 27342–27350. [CrossRef]
- 132. Li, H.; Jiang, N.; Li, J.; Huang, J.; Kong, J.; Xiong, D. Hard and tough (NbTaMoW)Nx high entropy nitride films with substoichiometric nitrogen. *J. Alloys Compd.* **2021**, *889*, 161713. [CrossRef]
- 133. Lai, C.-H.; Cheng, K.-H.; Lin, S.-J.; Yeh, J.-W. Mechanical and tribological properties of multi-element (AlCrTaTiZr)N coatings. *Surf. Coat. Technol.* **2008**, 202, 3732–3738. [CrossRef]
- 134. Nemchenko, U.S.; Beresnev, V.M.; Klimenko, S.A.; Podchernyaeva, I.A.; Turbin, P.V.; Andreev, A.A. Wear resistance of the multicomponent coatings of the (Ti-Zr-Hf-V-Nb-Ta)N system at elevated temperature. *J. Superhard Mater.* **2015**, 37, 322–326. [CrossRef]
- 135. Archard, J.F. Contact and Rubbing of Flat Surfaces. J. Appl. Phys. 1953, 24, 981–988. [CrossRef]
- 136. Ju, H. High-temperature self-lubricating metal nitride-based nanostructure composite films. In *Friction, Lubrication and Wear*; Chowdhury, M.A., Ed.; IntechOpen: London, UK, 2019.

Metals **2022**, 12, 847 21 of 23

137. Magnéli, A. Structures of the ReO<sub>3</sub>-type with recurrent dislocations of atoms: 'homologous series' of molybdenum and tungsten oxides. *Acta Cryst.* **1953**, *6*, 495–500. [CrossRef]

- 138. Xu, J.; Luo, H.; Ju, H.; Yu, L.; Zhou, G. Microstructure, mechanical and tribological properties of TaWN composite films. *Vacuum* **2017**, *146*, 246–251. [CrossRef]
- 139. Xu, J.; Ju, H.; Yu, L. Microstructure, oxidation resistance, mechanical and tribological properties of Mo–Al–N films by reactive magnetron sputtering. *Vacuum* **2014**, *103*, 21–27. [CrossRef]
- 140. Tao, H.; Tsai, M.T.; Chen, H.-W.; Huang, J.C.; Duh, J.-G. Improving high-temperature tribological characteristics on nanocomposite CrAlSiN coating by Mo doping. *Surf. Coat. Technol.* **2018**, 349, 752–756. [CrossRef]
- 141. Gassner, G.; Mayrhofer, P.H.; Kutschej, K.; Mitterer, C.; Kathrein, M. Magnéli phase formation of PVD Mo–N and W–N coatings. *Surf. Coat. Technol.* **2006**, 201, 3335–3341. [CrossRef]
- 142. Lo, W.-L.; Hsu, S.-Y.; Lin, Y.-C.; Tsai, S.-Y.; Lai, Y.-T.; Duh, J.-G. Improvement of high entropy alloy nitride coatings (AlCrNb-SiTiMo)N on mechanical and high temperature tribological properties by tuning substrate bias. *Surf. Coat. Technol.* 2020, 401, 126247. [CrossRef]
- 143. Braic, V.; Vladescu, A.; Balaceanu, M.; Luculescu, C.R.; Braic, M. Nanostructured multi-element (TiZrNbHfTa)N and (TiZrNbHfTa)C hard coatings. *Surf. Coat. Technol.* **2012**, 211, 117–121. [CrossRef]
- 144. Polcar, T.; Martinez, R.; Vítů, T.; Kopecký, L.; Rodriguez, R.; Cavaleiro, A. High temperature tribology of CrN and multilayered Cr/CrN coatings. *Surf. Coat. Technol.* **2009**, 203, 3254–3259. [CrossRef]
- 145. Polcar, T.; Cavaleiro, A. High-temperature tribological properties of CrAlN, CrAlSiN and AlCrSiN coatings. *Surf. Coat. Technol.* **2011**, 206, 1244–1251. [CrossRef]
- 146. Niu, R.; Li, J.; Wang, Y.; Chen, J.; Xue, Q. Structure and high temperature tribological behavior of TiAlN/nitride duplex treated coatings on Ti<sub>6</sub>Al<sub>4</sub>V. *Surf. Coat. Technol.* **2017**, 309, 232–241. [CrossRef]
- 147. He, N.; Li, H.; Ji, L.; Liu, X.; Zhou, H.; Chen, J. High temperature tribological properties of TiAlSiN coatings produced by hybrid PVD technology. *Tribol. Int.* **2016**, *98*, 133–143. [CrossRef]
- 148. Kim, C.W.; Kim, K.H. Anti-oxidation properties of TiAlN film prepared by plasma-assisted chemical vapor deposition and roles of Al. *Thin Solid Films* **1997**, *307*, 113–119. [CrossRef]
- 149. Musil, J.; Daniel, R.; Soldán, J.; Zeman, P. Properties of reactively sputtered W–Si–N films. Surf. Coat. Technol. 2006, 200, 3886–3895. [CrossRef]
- 150. Chawla, V.; Chawla, A.; Sidhu, B.S.; Prakash, S.; Puri, D. Oxidation Behavior of Nanostructured TiAlN and AlCrN Thin Coatings on ASTM-SA213-T-22 Boiler Steel. *J. Miner. Mater. Charact. Eng.* **2010**, *09*, 1037–1057. [CrossRef]
- 151. Li, M.-S.; Feng, C.-J.; Yang, G.-L.; He, X.-M.; Li, W.-K.; Xiang, J.-H. Oxidation resistance of (Ti,Al,Cr)N coatings at 800 °C. *Trans. Nonferrous Met. Soc. China* **2007**, *17*, s831–s834.
- 152. Tsai, D.-C.; Chang, Z.-C.; Kuo, L.-Y.; Lin, T.-J.; Lin, T.-N.; Shiao, M.-H.; Shieu, F.S. Oxidation resistance and structural evolution of (TiVCrZrHf)N coatings. *Thin Solid Films* **2013**, 544, 580–587. [CrossRef]
- 153. Wittmer, M.; Noser, J.; Melchior, H. Oxidation kinetics of TiN thin films. J. Appl. Phys. 1981, 52, 6659–6664. [CrossRef]
- 154. Ahlgren, M.; Blomqvist, H. Influence of bias variation on residual stress and texture in TiAlN PVD coatings. *Surf. Coat. Technol.* **2005**, 200, 157–160. [CrossRef]
- 155. Hsueh, H.-T.; Shen, W.-J.; Tsai, M.-H.; Yeh, J.-W. Effect of nitrogen content and substrate bias on mechanical and corrosion properties of high-entropy films (AlCrSiTiZr)<sub>100-x</sub>N<sub>x</sub>. *Surf. Coat. Technol.* **2012**, 206, 4106–4112. [CrossRef]
- 156. Lee, C.-Y.; Chien, C.-H.; Yeh, J.-W.; Lin, S.-J. Effects of the carbon-to-nitrogen ratio on the microstructure and properties of (CrNbSiTiZr)C N high-entropy carbonitride films. *Mater. Chem. Phys.* **2022**, 277, 125374. [CrossRef]
- 157. Lin, S.-Y.; Chang, S.-Y.; Chang, C.-J.; Huang, Y.-C. Nanomechanical Properties and Deformation Behaviors of Multi-Component (AlCrTaTiZr)NxSiy High-Entropy Coatings. *Entropy* **2013**, *16*, 405–417. [CrossRef]
- 158. Tsai, D.-C.; Chang, Z.-C.; Kuo, B.-H.; Shiao, M.-H.; Chang, S.-Y.; Shieu, F.-S. Structural morphology and characterization of (AlCrMoTaTi)N coating deposited via magnetron sputtering. *Appl. Surf. Sci.* **2013**, *282*, 789–797. [CrossRef]
- 159. Lai, C.-H.; Lin, S.-J.; Yeh, J.-W.; Chang, S.-Y. Preparation and characterization of AlCrTaTiZr multi-element nitride coatings. *Surf. Coat. Technol.* **2006**, 201, 3275–3280. [CrossRef]
- 160. Tsai, D.-C.; Liang, S.-C.; Chang, Z.-C.; Lin, T.-N.; Shiao, M.-H.; Shieu, F.-S. Effects of substrate bias on structure and mechanical properties of (TiVCrZrHf)N coatings. *Surf. Coat. Technol.* **2012**, 207, 293–299. [CrossRef]
- 161. Chang, H.-W.; Huang, P.-K.; Yeh, J.-W.; Davison, A.; Tsau, C.-H.; Yang, C.-C. Influence of substrate bias, deposition temperature and post-deposition annealing on the structure and properties of multi-principal-component (AlCrMoSiTi)N coatings. *Surf. Coat. Technol.* 2008, 202, 3360–3366. [CrossRef]
- 162. Cheng, K.-H.; Weng, C.-H.; Lai, C.-H.; Lin, S.-J. Study on adhesion and wear resistance of multi-element (AlCrTaTiZr)N coatings. *Thin Solid Films* **2009**, 517, 4989–4993. [CrossRef]
- 163. Hsieh, M.-H.; Tsai, M.-H.; Shen, W.-J.; Yeh, J.-W. Structure and properties of two Al–Cr–Nb–Si–Ti high-entropy nitride coatings. *Surf. Coat. Technol.* **2013**, 221, 118–123. [CrossRef]
- 164. Tsai, M.-H.; Yeh, J.-W.; Gan, J.-Y. Diffusion barrier properties of AlMoNbSiTaTiVZr high-entropy alloy layer between copper and silicon. *Thin Solid Films* **2008**, *516*, 5527–5530. [CrossRef]
- 165. Wang, W.; Zheng, S.; Pu, J.; Cai, Z.; Wang, H.; Wang, L.; He, G. Microstructure, mechanical and tribological properties of Mo-V-N films by reactive magnetron sputtering. *Surf. Coat. Technol.* **2020**, *387*, 125532. [CrossRef]

Metals **2022**, 12, 847 22 of 23

166. Barshilia, H.C.; Deepthi, B.; Rajam, K.S. Growth and characterization of aluminum nitride coatings prepared by pulsed-direct current reactive unbalanced magnetron sputtering. *Thin Solid Films* **2008**, *516*, 4168–4174. [CrossRef]

- 167. Choudhary, R.K.; Mishra, S.C.; Mishra, P.; Limaye, P.K.; Singh, K. Mechanical and tribological properties of crystalline aluminum nitride coatings deposited on stainless steel by magnetron sputtering. *J. Nucl. Mater.* **2015**, *466*, 69–79. [CrossRef]
- 168. Freitas, F.G.R.; Hübler, R.; Soares, G.; Conceição, A.G.S.; Vitória, E.R.; Carvalho, R.G.; Tentardini, E.K. Structural and Mechanical Properties of Zr-Si-N Thin Films Prepared by Reactive Magnetron Sputtering. *Mater. Res.* **2015**, *18*, 30–34. [CrossRef]
- 169. Chun, S.-Y.; Im, H.-H. Crystal Structure, Microstructure and Mechanical Properties of NbN Coatings Deposited by Asymmetric Bipolar Pulsed DC Sputtering. *J. Korean Ceram. Soc.* **2017**, *54*, 33–37. [CrossRef]
- 170. Barhai, P.K.; Kumari, N.; Banerjee, I.; Pabi, S.K.; Mahapatra, S.K. Study of the effect of plasma current density on the formation of titanium nitride and titanium oxynitride thin films prepared by reactive DC magnetron sputtering. *Vacuum* **2010**, *84*, 896–901. [CrossRef]
- 171. Bouaouina, B.; Besnard, A.; Abaidia, S.E.; Airoudj, A.; Bensouici, F. Correlation between mechanical and microstructural properties of molybdenum nitride thin films deposited on silicon by reactive R.F. magnetron discharge. *Surf. Coat. Technol.* 2018, 333, 32–38. [CrossRef]
- 172. Yeung, W.Y.; Dub, S.N.; Wuhrer, R.; Milman, Y.V. A nanoindentation study of magnetron co-sputtered nanocrystalline ternary nitride coatings. *Sci. Sinter.* **2006**, *38*, 211–221. [CrossRef]
- 173. Ramadoss, R.; Kumar, N.; Pandian, R.; Dash, S.; Ravindran, T.R.; Arivuoli, D.; Tyagi, A. Tribological properties and deformation mechanism of TiAlN coating sliding with various counterbodies. *Tribol. Int.* **2013**, *66*, 143–149. [CrossRef]
- 174. Shypylenko, A.; Pshyk, A.V.; Grześkowiak, B.; Medjanik, K.; Peplinska, B.; Oyoshi, K.; Pogrebnjak, A.; Jurga, S.; Coy, E. Effect of ion implantation on the physical and mechanical properties of Ti-Si-N multifunctional coatings for biomedical applications. *Mater. Des.* **2016**, *110*, 821–829. [CrossRef]
- 175. Ait-Djafer, A.Z.; Saoula, N.; Aknouche, H.; Guedouar, B.; Madaoui, N. Deposition and characterization of titanium aluminum nitride coatings prepared by RF magnetron sputtering. *Appl. Surf. Sci.* **2015**, *350*, 6–9. [CrossRef]
- 176. Yang, Q. Wear resistance and solid lubricity of molybdenum-containing nitride coatings deposited by cathodic arc evaporation. *Surf. Coat. Technol.* **2017**, 332, 283–295. [CrossRef]
- 177. Aouadi, S.M.; Wong, K.C.; Mitchell, K.A.R.; Namavar, F.; Tobin, E.; Mihut, D.M.; Rohde, S.L. Characterization of titanium chromium nitride nanocomposite protective coatings. *Appl. Surf. Sci.* **2004**, 229, 387–394. [CrossRef]
- 178. Castanho, J.M.; Vieira, M.T. Effect of ductile layers in mechanical behaviour of TiAlN thin coatings. *J. Mater. Process. Technol.* **2003**, 143–144, 352–357. [CrossRef]
- 179. Yang, Q.; Zhao, L.R.; Patnaik, P.C.; Zeng, X.T. Wear resistant TiMoN coatings deposited by magnetron sputtering. *Wear* **2006**, 261, 119–125. [CrossRef]
- 180. Mo, J.L.; Zhu, M.H.; Lei, B.; Leng, Y.X.; Huang, N. Comparison of tribological behaviours of AlCrN and TiAlN coatings—Deposited by physical vapor deposition. *Wear* 2007, 263, 1423–1429. [CrossRef]
- 181. Chang, C.-L.; Lin, C.-T.; Tsai, P.-C.; Ho, W.-Y.; Wang, D.-Y. Influence of bias voltages on the structure and wear properties of TiSiN coating synthesized by cathodic arc plasma evaporation. *Thin Solid Films* **2008**, *516*, 5324–5329. [CrossRef]
- 182. Yang, S.; Li, X.; Cooke, K.E.; Teer, D.G. A study of TiMoN nano-multilayer coatings deposited by CFUBMSIP using DC and HIPIMS power. *Appl. Surf. Sci.* **2012**, 258, 2062–2067. [CrossRef]
- 183. Uglov, V.V.; Anishchik, V.M.; Zlotski, S.V.; Abadias, G.; Dub, S.N. Stress and mechanical properties of Ti–Cr–N gradient coatings deposited by vacuum arc. *Surf. Coat. Technol.* **2005**, 200, 178–181. [CrossRef]
- 184. Lin, Y.-W.; Chen, H.-A.; Yu, G.-P.; Huang, J.-H. Effect of bias on the structure and properties of TiZrN thin films deposited by unbalanced magnetron sputtering. *Thin Solid Films* **2016**, *618*, 13–20. [CrossRef]
- 185. Ren, B.; Shen, Z.; Liu, Z. Structure and mechanical properties of multi-element (AlCrMnMoNiZr)Nx coatings by reactive magnetron sputtering. *J. Alloys Compd.* **2013**, *560*, 171–176. [CrossRef]
- 186. Chen, T.-K.; Wong, M.-S.; Shun, T.-T.; Yeh, J.-W. Nanostructured nitride films of multi-element high-entropy alloys by reactive DC sputtering. *Surf. Coat. Technol.* **2005**, 200, 1361–1365. [CrossRef]
- 187. Zhang, Y.; Yan, X.-H.; Liao, W.-B.; Zhao, K. Effects of Nitrogen Content on the Structure and Mechanical Properties of (Al<sub>0.5</sub>CrFeNiTi<sub>0.25</sub>)N<sub>x</sub> High-Entropy Films by Reactive Sputtering. *Entropy* **2018**, 20, 624. [CrossRef]
- 188. Kim, Y.S.; Park, H.J.; Mun, S.C.; Jumaev, E.; Hong, S.H.; Song, G.; Kim, J.T.; Park, Y.K.; Kim, K.S.; Jeong, S.I.; et al. Investigation of structure and mechanical properties of TiZrHfNiCuCo high entropy alloy thin films synthesized by magnetron sputtering. *J. Alloys Compd.* **2019**, 797, 834–841. [CrossRef]
- 189. Rogström, L.; Johansson-Jõesaar, M.P.; Landälv, L.; Ahlgren, M.; Odén, M. Wear behavior of ZrAlN coated cutting tools during turning. *Surf. Coat. Technol.* **2015**, *282*, 180–187. [CrossRef]
- 190. Liu, Z.; An, Q.; Xu, J.; Chen, M.; Han, S. Wear performance of (nc-AlTiN)/(a-Si<sub>3</sub>N<sub>4</sub>) coating and (nc-AlCrN)/(a-Si<sub>3</sub>N<sub>4</sub>) coating in high-speed machining of titanium alloys under dry and minimum quantity lubrication (MQL) conditions. *Wear* **2013**, 305, 249–259. [CrossRef]
- 191. Fox-Rabinovich, G.S.; Kovalev, A.I.; Aguirre, M.H.; Beake, B.D.; Yamamoto, K.; Veldhuis, S.C.; Endrino, J.L.; Wainstein, D.L.; Rashkovskiy, A.Y. Design and performance of AlTiN and TiAlCrN PVD coatings for machining of hard to cut materials. *Surf. Coat. Technol.* **2009**, 204, 489–496. [CrossRef]

Metals **2022**, 12, 847 23 of 23

192. Tsai, D.-C.; Chang, Z.-C.; Kuo, B.-H.; Tsao, C.-T.; Chen, E.-C.; Shieu, F.-S. Influence of discharge power on the structural, electro-optical, and mechanical properties of (TiZrHf)N coatings. *J. Alloys Compd.* **2015**, 622, 446–457. [CrossRef]

193. Özkan, D.; Yılmaz, M.A.; Szala, M.; Türküz, C.; Chocyk, D.; Tunç, C.; Göz, O.; Walczak, M.; Pasierbiewicz, K.; Yağcı, M.B. Effects of ceramic-based CrN, TiN, and AlCrN interlayers on wear and friction behaviors of AlTiSiN + TiSiN PVD coatings. *Ceram. Int.* **2021**, *47*, 20077–20089. [CrossRef]